Tunnel Mechanisms and Junction Characterization in III-V Tunnel Diodes*

A. M. Andrews, H. W. Korb,† and N. Holonyak, Jr.
Department of Electrical Engineering and Materials Research Laboratory, University of Illinois at Urbana-Champaign, Urbana, Illinois 61801
and
C. B. Duke and G. G. Kleiman
Department of Physics, Materials Research Laboratory, and Coordinated Science Laboratory, University of Illinois at Urbana-Champaign, Urbana, Illinois 61801
(Received 13 September 1971)

Via a study of alloy tunnel diodes on GaAs: Zn substrates, we conclude that at high substrate doping levels, $p \gtrsim 5\times10^{19}$ cm^{-3}, average-barrier tunneling predominates, whereas at lower substrate dopings, $p \lesssim 1.3\times10^{19}$ cm^{-3}, impurity-assisted tunneling predominates. The photosensitive features of the tunneling characteristics in units made on the more lightly doped substrates permit us to identify both elastic and inelastic resonant ("two-step") tunneling processes associated with Au-Ge traps in the space-charge region. A summary of the predictions of a microscopic theory of resonant tunneling is presented and used to interpret both our own data and those already extant in the literature. The qualitative features of the predictions of this theory permit us to characterize defect structures and optical-phonon energies in III-V mixed-crystal alloy diodes on $Ga_{1-x}Al_xAs$, $GaAs_{1-x}P_x$, and $In_{1-x}Ga_xP$. This characterization indicates that in ternary crystals whose binary components exhibit appreciable lattice mismatch, alloy regrowth introduces numerous additional defects, and in some systems, like $In_{1-x}Ga_xP$, even the introduction of high acceptor densities disorders the crystal lattice. Such defects cause pronounced minima near zero bias in the tunnel conductance.

I. INTRODUCTION

After almost two decades of extensive studies of tunneling in semiconductors,[1,2] in the past two years a new concept has begun to emerge: that the dominant mechanism of electron tunneling depends explicitly on the potential-energy profile in the junction (i.e., the thickness and defect structure of the junction and chemistry of the dopants). Three distinct "ranges" of tunneling phenomena have been identified in junctions on GaAs substrates. At "high" substrate doping for either metal contacts or p-n diodes, the tunneling barrier acts like the average one-electron potential, as is commonly regarded to be the case.[1-5] At a somewhat lower substrate doping, the tunneling becomes "two-step" in nature[6,7] with the carriers traversing the junction by way of real intermediate states in the barrier.[8-11] Finally, at dopings sufficiently low that the "metal-insulator" transition in the bulk semiconductor is approached ($n \sim n_c$ in the notation of Alexander and Holcomb[12]), the two-step mechanism merges into an impurity-band conduction mechanism.[13,14] It is an interesting but untested hypothesis that the change from two-step to average-barrier tunneling occurs at the "impurity-band–free-electron" transition, $n \cong n_{cb}$. This hypothesis is consistent with existing data.[3,4,8,12-14] If applied to the units described herein it would imply $1.29\times10^{19} < p_{cb} < 5.4\times10^{19}$ cm^{-3} for the free-hole–impurity-band critical concentration p_{cb} in GaAs: Zn.

Still more recently[15-18] a second new concept has been proposed: that resonant impurity-assisted (i.e., "two-step") elastic tunneling is accompanied by characteristic manifestations in inelastic-tunneling channels (most notably associated with phonons). Although it is too early to determine definitively the fate of this proposal, it does describe a relationship between zero-bias conductance minima and large forward-reverse-bias asymmetries which have been observed in many p-n junctions[1,8,19-22] and metal-semiconductor contacts.[1,8,9,12,13,23-31]

The purpose of this paper is the presentation of a test of these two new concepts in GaAs tunnel diodes, and their subsequent application to characterize diodes in the III-V mixed-crystal compounds $GaAs_{1-x}P_x$, $Ga_{1-x}Al_xAs$, and $In_{1-x}Ga_xP$. Following a discussion of experimental methods in Sec. II, we present in Sec. III one test of the model concepts by virtue of a study of photosensitive tunneling in GaAs p-n junctions and metal-semiconductor contacts. Our main results in Sec. III are the demonstrations that for Zn substrate dopings of $p \cong 5.4\times10^{19}$ cm^{-3} predictions of the one-electron average-barrier model adequately describe the data, whereas for substrate dopings $p \cong 1.3\times10^{19}$ cm^{-3} the two-step tunneling mechanism is both necessary and sufficient to explain the wide variety of observations. We do not examine substrates which are sufficiently lightly doped ($p \lesssim 8\times10^{18}$ cm^{-3}) that impurity-band phenomena are expected to become important.[14]

Having documented in Sec. III the manifestations

of various tunneling mechanisms, in Sec. IV we apply this insight to characterize p-n junctions fabricated from mixed-crystal systems[32] ($Ga_{1-x}Al_xAs$, $GaAs_{1-x}P_x$, and $In_{1-x}Ga_xP$). Examining first the elastic-tunneling current as an indication of the defect structure in the junction, we find that as we go from $Ga_{1-x}Al_xAs$ to $In_{1-x}Ga_xP$, the increasing lattice mismatch between the two compounds in the mixed crystal (e.g., GaAs and AlAs in $Ga_{1-x}Al_xAs$) causes increasing concentrations of defects in the junction region. Given comparable fabrication methods, these defects make the construction of "good" (i.e., average-barrier) tunnel diodes progressively more difficult until in $In_{1-x}Ga_xP$ the impurity- (defect-) assisted current dominates the diode characteristics at all values of the bias. In Sec. IV we also apply the results of previous analyses[1,33-35] of phonon-induced electronic-self-energy phenomena to measure optical-phonon energies as a function of alloy composition in the mixed-crystal diodes.

Finally in Sec. V we turn to an additional verification of the "two-step" nature of tunneling in intermediate-doped semiconductors: the demonstration of the experimental realization of a predicted relationship[17,18] between the elastic- and phonon-assisted-tunneling processes for situations in which "two-step" tunneling predominates. Using a new theory[17,18] which simultaneously describes resonant- and many-body-tunneling phenomena, a model of resonant tunneling[36] through vibrating impurity quasibound states in the junction is analyzed. The resonant-elastic tunneling is a microscopic analog of the semiempirical "two-step" tunneling mechanism.[6,7] The new prediction of the theory is the existence of comparable effects in the electronic proper self-energies. These in turn are manifested as structure in the conductance at the impurity-local-mode or optical-phonon energies depending on the properties of the host material and the impurity. Such effects cause large (observed) forward-reverse-bias asymmetries in the fine structure in the tunnel characteristics at the appropriate phonon energy. Therefore their observation in our experimental studies both confirms the basic features of a new theory of tunneling, and adds a further means of characterizing the mechanisms of current flow in tunnel junctions.

Our conclusions are summarized in Sec. VI. In brief, we feel that we have altered fundamental ideas about the nature of tunneling in compound semiconductor junctions. The conduction process is determined by a competition between impurity-assisted tunneling at low substrate dopings and average-barrier tunneling at high doping. In particular, the dominant mechanism of current flow near zero bias in moderately and lightly doped units is resonant-elastic tunneling. Finally, the extension of such ideas about the dependence of both elastic- and inelastic-tunneling mechanisms on the impurity concentration permits us to apply tunneling as a technique for characterizing new materials.

II. EXPERIMENTAL METHODS

The semiconductor crystals used in this work (GaAs, $Ga_{1-x}Al_xAs$, $GaAs_{1-x}P_x$, and $In_{1-x}Ga_xP$) were purchased or grown in our laboratory. The Zn-doped and the semi-insulating GaAs substrate material were obtained from the Monsanto Corp. GaAs layers containing Au and Ge for electrical and optical measurements, photoconductivity experiments, and metal-semiconductor (MS) contact fabrication were grown on GaAs substrates by liquid-phase epitaxy from a melt of Au-Sb eutectic containing a few percent Ge and saturated with GaAs at the growth temperature of 600 °C. The substrates were n type if Ohmic contacts to the entire epitaxial layers were desired, as for MS contact fabrication. They were semi-insulating for photoconductivity and Hall measurements. Standard Hall and van der Pauw measurements were used to determine dopings and mobilities.

The $Ga_{1-x}Al_xAs$ samples were grown on heavily Zn-doped GaAs substrates by liquid-phase epitaxy from a Zn-doped Ga melt saturated with GaAs at the growth temperature of 800 °C and with an appropriate amount of Al to give the desired Al : Ga ratio. During the growth cycle, as the Al in the melt depleted, the Al : Ga ratio of the grown layer steadily decreased. The thickness of the epitaxial layers was about 70 μ. A range of Al content for tunnel-diode fabrication was obtained by lapping and polishing various pieces of the grown layer to different depths. The Al content was determined by electron-microprobe analysis. The penetration depth of the electron beam was about 1 μ, so the composition measured was that near the surface where the tunnel junction was formed. The Zn concentration was obtained from a Hall measurement on a sample grown on a semi-insulating substrate.

The $GaAs_{1-x}P_x$ crystals were grown by halogen-vapor transport in sealed quartz ampoules.[37] Some of the crystals were doped with Zn during the growth process, while the remainder were doped by Zn diffusion of thin wafers in a sealed ampoule.[38] The lower P compositions, in the direct material, were determined from the wavelength of recombination radiation excited in the crystals. The higher P compositions were determined from the relative amounts of constituents placed in the growth ampoule.

A modified Bridgman solution-growth technique[39] was used to grow the $In_{1-x}Ga_xP$ crystals. Some crystals were grown from Zn doping, and others were grown with Te doping and then were doped p-

type by Zn diffusion. Doping levels were determined from Hall measurements. The Ga content of the crystals was determined by electron-microprobe analysis.

Tunnel diodes were fabricated by an alloy regrowth process carried out on a strip heater in a hydrogen atmosphere. First, the polished p-type crystal substrate was alloyed to a header. Then an alloy dot containing the donor dopant (as well as any other impurities desired, such as Au) was placed on the substrate and the assembly was heated until the alloy melted and dissolved a small portion of the crystal. The system was then cooled rapidly, producing an n-type regrown region and an abrupt p-n junction. A thin Ni lead was connected to the alloy dot and was soldered to the header lead. Large area junctions in GaAs, $GaAs_{1-x}P_x$, and $Ga_{1-x}Al_xAs$ were reduced in size in a NaOH electrolytic etch until a size which produced a convenient current level was reached. Capacitance measurements were made on a variety of junctions, and plots of $1/C^2$ vs V were linear, confirming that abrupt junctions were obtained.

MS contacts were fabricated on a number of Au-Ge–doped GaAs epitaxial layers, on both as-grown and etched surfaces. The surfaces were outgassed in vacuum at 400 °C for 10 min prior to evaporation of a thick Pb film through a mask. A thinner Au film was then evaporated and served to protect the Pb film against mechanical damage from pressure contacts.

Electrical measurements on the p-n junctions and MS contacts included recorder plots of the I-V characteristics, dI/dV, and, where appropriate, d^2I/dV^2. The derivatives were measured by superimposing a small ac signal on the dc bias and measuring the components of current at the fundamental and second-harmonic frequencies. These currents are proportional to dI/dV and d^2I/dV^2, respectively. While this procedure for measuring derivatives of I-V characteristics is well known,[40] the circuit used incorporates some special features useful for this set of experiments and is to be described elsewhere.[41] Of particular interest are the capability for measurement in the negative resistance region of p-n tunnel diodes and an arrangement for automatic compensation for second-harmonic components in the modulation signal.

The measurements were generally made with the devices immersed in liquid helium at 4.2 °K. Measurements at other temperatures were made in a variable-temperature cryostat. During measurements on the Pb-GaAs contacts, provisions were made to quench the superconductivity of the Pb contact by applying a magnetic field.

The photoresponse of the GaAs (Zn : Au-Ge) tunnel diodes and epitaxial Au-Ge–doped GaAs layers to be described in Sec. III were measured by establishing the diode at the proper temperature, applying a particular bias, and measuring the response to chopped nearly monochromatic light. The light source was a Pek Labs 100-W mercury-arc lamp whose output was chopped at 1–2 Hz and fed into a Bausch & Lomb grating monochromator. One end of a fiber light pipe was mounted on the monochromator output and the other end was mounted in close proximity to the device, resulting in efficient transfer of the light signal to the device. The ac component of the current was detected with a PAR 124 lock-in amplifier synchronized to the frequency of the chopped light.

To detect any long-wavelength emission from the GaAs (Zn : Au-Ge) tunnel diodes, a Ge : Hg detector with a detectivity of $\sim 10^{10}$ cm $Hz^{1/2}/W$ (4.2 °K) at 8 μ was employed. The detector and its MOSFET preamplifier were held at liquid-helium temperature along with the tunnel diode which was placed in close proximity to the face of the detector. The tunnel diode was biased at the voltage where maxima in photoexcited currents occur, and a 300-mV (peak-to-peak) signal at 5–100 Hz was superimposed on the dc bias of the diodes so as to sweep through the bias range of the inelastic current channel. The output of the detector preamplifier was measured with a PAR 124 lock-in amplifier synchronized in turn to the signal frequency and to twice the signal frequency. As each cycle of the modulation signal swept the voltage through the region of peak excess current twice, the light output would be expected to occur at twice the signal frequency. Measurements were taken before and after the excitation of the excess-current channel.

Noise currents in tunnel diodes were measured by placing a resistor in parallel with the diode to make the net conductance positive (thus preventing circuit oscillations), sweeping the diode bias slowly with a high-impedance source, and coupling the fluctuation currents into a simple low-impedance low-noise grounded-base preamplifier similar to one described by Copeland.[42] The signal was amplified and measured using the PAR 124 as an average-reading wideband voltmeter, and the wideband noise current was plotted on an XY recorder as a function of junction bias. The spectral density of the noise current at particular bias points was determined by operating the PAR 124 as a tuned amplifier of fixed Q and measuring the signal at a number of frequencies. The bandwidth at a center frequency f_0 was then proportional to f_0/Q. The background noise level of the measuring system is about 5×10^{-21} A^2/Hz.

The results obtained by these various measurements are described below.

III. TUNNELING IN Au-Ge ALLOY p-n JUNCTIONS ON GaAs(Zn)

The central issue to which we direct our attention

in this section is the determination of the tunneling mechanism as a function of the doping of the (p-type) substrate in GaAs p-n tunnel diodes. It has been known for many years that quantitative comparisons of the predictions of the one-electron average-barrier tunneling model with experimental data led to the observation of much larger current densities than predicted.[43] Only in the past few years has the model's predictions been shown to quantitatively describe any data: thus far, the tunnel characteristics of metal contacts on n-type Ge,[1,3,4] Si,[44] and CdS.[29] Consequently, our first task, accomplished in Sec. III A, is the verification that for p-n diodes, as well as MS contacts, predictions based on the average-barrier model quantitatively describe the tunneling data for an appropriate range of dopings ($p \sim 5\times10^{19}$ cm^{-3}; $n \simeq 1.5\times10^{19}$ cm^{-3}). We quickly discovered, however, that p-n diodes made using the same fabrication technique on more lightly doped substrates [$p \simeq (1.3\text{–}2.4)\times10^{19}$ cm^{-3}] did not yield tunnel characteristics in agreement with the predictions of the average-barrier model and, in addition, exhibited strongly photosensitive characteristics.[9,45] The photosensitivity of the tunnel current provides a unique probe of the mechanisms of tunneling, a fact which we exploit in Sec. III B to establish impurity-assisted tunneling, both resonant[36] and nonresonant,[1] as the dominant tunneling mechanisms in units made on these more lightly doped substrates. In Sec. III C we note that a prominent photosensitive impurity-assisted inelastic-tunneling process in these units[45] also is associated with a large noise current. In Sec. III D we relate our studies of p-n tunnel diodes to ones of the characteristics of MS contacts and the bulk properties of epitaxial layers of n-type GaAs : Au-Ge of material comparable to that in the alloy regrowth region of the p-n diodes. We conclude in Sec. III E with a summary of our composite model of tunneling in III-V semiconductors for use as a reference to characterize new materials by means of tunneling experiments.

A. Validity of One-Electron Theory: Tunneling in Heavily Zn-Doped GaAs

The devices were fabricated as described in Sec. II with a Au-Ge or Au-Sb eutectic doped with Ge alloyed on highly polished Zn-doped GaAs substrates, where for the heavily doped units $p = 5.4\times10^{19}$ cm^{-3} and for the lightly doped units $p = 1.3\times10^{19}$ cm^{-3}. The I-V and C-V data were obtained at 4.2 °K. According to the abrupt junction model[46] of a p-n diode, the capacitance in Gaussian units satisfies

$$\frac{1}{C^2} = \left(\frac{8\pi(p+n)}{eA^2\epsilon pn}\right)(V_c - V)\ . \tag{1}$$

In Eq. (1), n is the carrier concentration on the n side, A is the junction area, ϵ is the dielectric constant of GaAs (i.e., $\epsilon = 13$), and e is the electronic charge. We have assumed that all acceptors and donors are ionized [i.e., the donor (acceptor) concentration N_d (N_a) $= n$ (p)]. The carrier concentrations of the n-type regrown regions were obtained from the slope of the $1/C^2$-vs-V plot while junction areas were obtained from direct optical measurements.

The average-barrier tunneling current was calculated using the effective-mass approximation and assuming the bands on the two sides of the junction to be continuous across the n-p interface.[47] The potential energy of the electrons in this model is given by the following equation[47]:

$$\begin{aligned} V(x) &= V_B - eV, && x \geq d_p \\ &= -\frac{2\pi e^2}{\epsilon}\,p(x-d_p)^2 + V_B - eV, && 0 \leq x \leq d_p \\ &= \frac{2\pi e^2}{\epsilon}\,n(x+d_n)^2, && -d_n \leq x \leq 0 \\ &= 0, && x \leq -d_n\ . \end{aligned} \tag{2}$$

The widths of the p and n regions are represented by d_p and d_n, respectively. The quantity V_B is the height of the average barrier for a tunneling electron.

The junction thicknesses d_n and d_p are derived from the continuity of $V(x)$ and $\partial V/\partial x$ across the junction plane at $x = 0$:

$$pd_p^2 + nd_n^2 = \epsilon(V_B - eV)/2\pi e^2, \quad pd_p = nd_n\ . \tag{3}$$

Therefore from a knowledge of these n, p, and V_B, the barrier-penetration factor and the resulting average-barrier current for nonzero temperature can be calculated.[1,47]

In the abrupt-junction model of a p-n tunnel diode, the energy eV_c, for which $1/C^2$ is zero, is the barrier height. Extrapolations of our capacitance measurements on the highly doped units (i.e., $p = 5.4\times10^{19}$ cm^{-3}) indicate that eV_c is less than the band gap in GaAs, E_g (i.e., $E_g = 1.52$ eV at $T = 4.2$ °K). This result is amply documented in the literature.[48] It cannot be reconciled with the abrupt-junction model of the diode by including the effects of either mobile-carrier density[49] or impurity-induced conduction- and valence-band shifts.[50] The barrier height which is consistent with our model[47] satisfies

$$V_B = E_g + \xi_n + \xi_p\ ; \tag{4}$$

the quantities ξ_n and ξ_p are the Fermi degeneracies on the n and p sides, respectively.[47]

We have used Eqs. (1)–(4) to calculate the barrier-penetration probability and the concomitant current characteristics for nonzero temperature according to standard techniques.[47] Comparison of the one-electron theory of the average-barrier

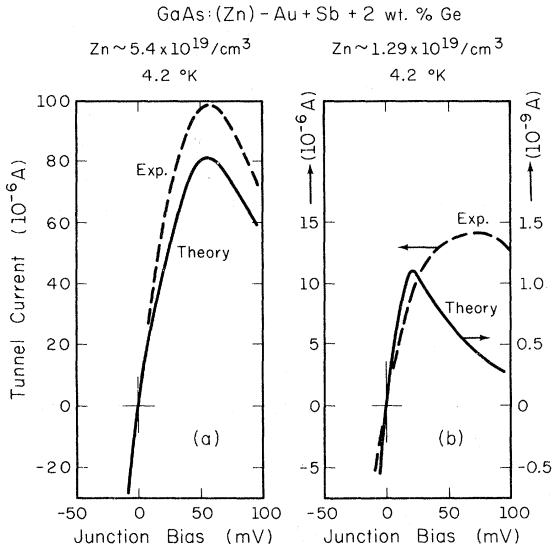

FIG. 1. Comparison between experimentally measured I-V and calculated one-electron average-barrier tunneling I-V at 4.2 °K. (a) Heavily doped ($Zn \sim 5.4\times10^{19}$ cm^{-3}) GaAs(Zn: Au-Ge) tunnel diode, with good agreement between theory and experiment. (b) Lightly doped ($Zn \sim 1.3\times10^{19}$ cm^{-3}) GaAs(Zn: Au-Ge) tunnel diode showing poor agreement between theory and experiment. The doping of the n-type alloy regrowth region and the magnitude of the built-in voltage were determined from capacitance measurements to be $n = 1.5\times10^{19}$ cm^{-3}, $V_B = 1.42$ eV and $n = 6\times10^{18}$ cm^{-3}, $V_B = 1.51$ eV in the two units, respectively. Their areas were determined visually to be 0.13×10^{-4} and 0.8×10^{-4} cm^2, respectively.

tunneling current with the experimental current of heavily Zn-doped units is shown in Fig. 1(a), and the comparison with the lightly doped units is shown in Fig. 1(b). In the heavily doped units, there is adequate agreement in the voltage positions of the maxima as well as in the magnitudes of the experimentally measured and theoretically calculated currents. The corresponding currents in the lightly doped units, on the other hand, differ in the voltage positions of their maxima; the most marked feature of Fig. 1(b), however, is the extreme discrepancy in the magnitudes of the theoretical and experimental currents. The only other recent fit to one-electron theory that has been applied with all of the model parameters determined independently on the same unit has been that of MS contacts on Ge.[3,4] Here, to within the uncertainties noted following Eq. (3), we have verified the validity of the one-electron theory for heavily Zn-doped GaAs tunnel diodes fabricated with special n-type alloys (i.e., Au-Ge or Au-Sb-Ge), and discounted its validity for the lightly doped diodes which are prepared in the same way. In the remainder of Sec. III, we examine the photosensitivity of the lightly doped units in order to determine the dominant current-flow mechanisms in these units.

B. Mechanism of Photosensitive Tunneling in Lightly Doped Units

Having shown that the average-barrier tunneling model fails to predict the magnitude of observed currents in lightly Zn-doped units, we investigate other possible tunneling mechanisms in these units. A variety of mechanisms of tunneling have been proposed for the "humps" in the valley current and excess tunneling current,[51] but only average-barrier tunneling has been assumed for the low-bias range.[43,52] From studies of photosensitive GaAs tunnel diodes,[9,45] we eliminate average-barrier tunneling as the dominant current mechanism and attribute the zero-bias conductance minima to resonant-elastic tunneling through impurity or defect-trap states in the barrier.

The junction-fabrication technique has already been described. The n-type alloys were those grown with Au-Ge eutectics. A Au-Ge complex is thought to be responsible for the photosensitive effects observed in the lightly doped diodes because it is only the combined presence of Au and Ge in an n-type alloy system that produces the effect. The GaAs substrates investigated showing strong photosensitivity were Zn doped in the range $9\times10^{18} \leq p \leq 2.4\times10^{19}$ cm^{-3}.

The curve-tracer plot shown in Fig. 2 shows a typical I-V characteristic at 77 °K. The lower trace is the I-V characteristic before any excitation, and the upper trace is the I-V characteristic after excitation. This excitation can be accomplished with either light of a particular wavelength or bias above 0.5 V. Once the diode has been excited, it retains its excited I-V characteristic at 4.2 °K for periods as long as several hours. Figure 3 shows the 77 °K current response, at 260-mV bias, to chopped

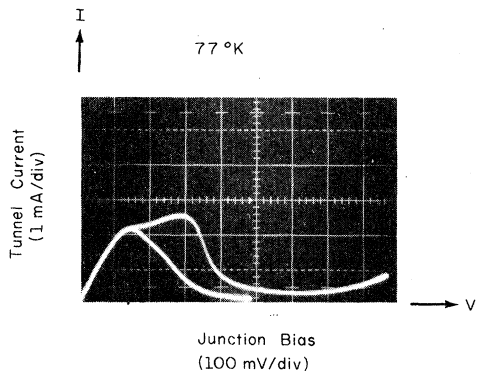

FIG. 2. I-V curve-tracer plot at 77 °K of a GaAs(Zn: Au-Ge) tunnel diode. The lower trace is obtained in the dark. The upper trace is obtained after saturation of changes in characteristics with the radiation output of a tungsten lamp.

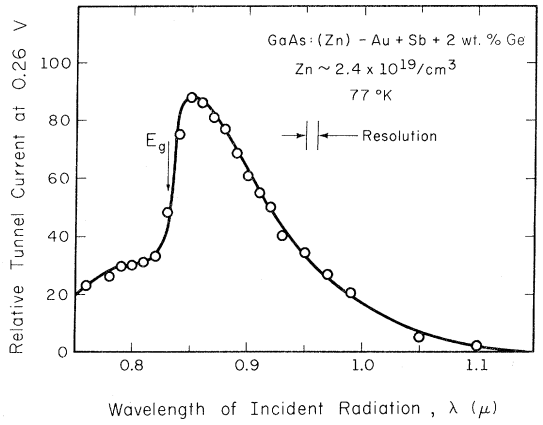

FIG. 3. Photoresponse of a GaAs(Zn:Au-Ge) tunnel diode at 77 °K biased at 260 mV, to various wavelengths of chopped radiation.

radiation of various wavelengths. These data indicate a photoactivation energy of the Au-Ge center of $E_a \simeq 1.36$ eV. From the thermal decay of the photoexcited excess current we find a thermal deactivation energy of (140 ± 20) meV for the Au-Ge complex to revert back to its unexcited condition.

Because the bias at which the excess photosensitive current occurs lies in the negative resistance region of the I-V characteristic, we interpret this current to be a tunneling phenomenon. A line-shape analysis[45] indicated this to be an inelastic-tunneling process rather than a space-charge effect[53,54] or resonant-elastic tunneling.[36,55] The excitation energy of the inelastic-tunneling mechanism was found to be $E_{exc} = (150 \pm 10)$ meV. As this is an energy-loss mechanism associated with the excitation of an excited state in the barrier, the possibility of radiative relaxation of this excitation exists. We searched the long-wavelength region of the spectrum with a Ge : Hg detector (held at 4.2 °K) and did not detect any emission. Consequently the inelastic-tunneling excited state is assumed to be nonradiative.

In Fig. 4 we show I-V and G-V data taken at 4.2 °K in a typical lightly doped GaAs (Zn : Au-Ge) tunnel diode. A striking aspect of these data is the large photosensitive zero-bias conductance minimum. Also shown in Fig. 4 is the linear relationship between the decrease in the zero-bias conductance and the increase in the inelastic current at 260 meV as the junction is more heavily excited (i.e., as more Au-Ge defects are activated). This illustrates how the inelastic current is "turned on" while the zero-bias conductance is "turned off." This decrease in the conductance at zero bias cannot be explained as a space-charge effect. The capacitance of these diodes increases (by several percent) upon excitation, and for tunneling through an average barrier one would predict an increase in both $I(V \simeq 0)$ and $G(0)$ for a decrease in the average-barrier width. Thus average-barrier tunneling can be eliminated as the dominant current-carrying mechanism for small values of the bias. This observation is consistent with the fact that average-barrier tunneling calculations do not give, even within an order of magnitude, the currents observed in lightly doped units.

Another significant feature of the G-V data shown in Fig. 4 is the increase with increasing excitation of the width and depth of the conductance minimum near zero bias. This behavior is important in eliminating the numerous earlier interpretations of zero-bias conductance minima[9,19–25,56]; such effects cannot be accounted for by the density-of-states models[22–24,56] or by inelastic-tunneling models.[25] The density-of-states models are incompatible with the data since the various transport parameters of both the sub-

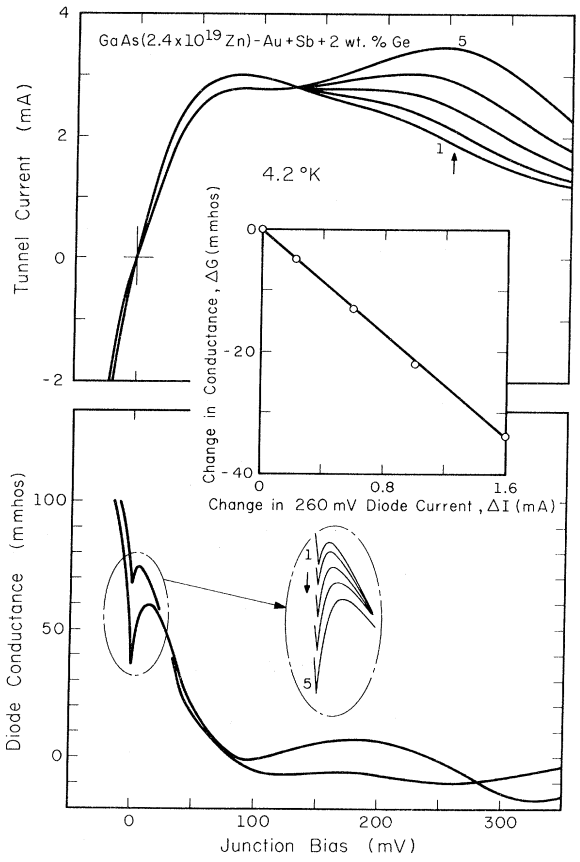

FIG. 4. I-V and G-V characteristics at 4.2 °K of a GaAs(Zn:Au-Ge) tunnel diode. The various curves in each panel indicate the characteristics for increasing levels of photoexcitation with the unexcited characteristics being denoted by 1. The inset shows the relation between the reduction in conductance at zero bias and the increase in current at a bias of 260 mV (after Duke *et al.*, Ref. 9).

strate GaAs and the epitaxial grown layers, Au-Ge doped, are light insensitive.[57] The inelastic-tunneling models predict a constant value of $G(V=0)$ and a light-independent width of the conductance minimum. Hence their relevance to the p-n tunneling data where both the width of the minimum and $G(0)$ depend on the photoexcitation cannot be established. Therefore, we argue that upon excitation the Au-Ge impurity supplies states near the Fermi energy in the barrier and that resonant-elastic tunneling via these states causes the zero-bias conductance minimum.

The $I(V)$ and $G(V)$ characteristics shown in Fig. 4 can be interpreted in terms of elastic- and inelastic-tunneling currents. For elastic tunneling we recall the three types of tunneling mechanisms: (i) average-barrier tunneling,[43] (ii) nonresonant impurity-assisted tunneling,[25] and (iii) resonant impurity-assisted tunneling.[36] As we have eliminated the average-barrier tunneling as a possible mechanism, we restrict our model to the impurity-assisted tunneling processes. The resonant-elastic tunneling also can be described as a "two-step" process[6-8] in which a tunneling electron hops onto a trap in the barrier and then hops off as it tunnels on through the barrier. Finally, the mechanism to which we attribute the photosensitive current is a change in the charge state of the Au-Ge complex induced by the incident photon.[9,45] If we assume, as seems most likely, that the complex is on the n-type side of the junction, this reaction can be expressed as

$$\mathrm{Au}^{(q+1)-} + h\nu \rightarrow \mathrm{Au}^{q-} + q \ , \tag{5}$$

where the "Au" symbolizes the Au-Ge trap and the photon energy is ~1.36 eV (the photoexcitation energy of the trap).

Our model of the low-bias tunneling involves three types of processes. In their "unexcited" charge state, n "Au" complexes support a nonresonant impurity-assisted elastic current $I \equiv nI_1^e(V)$. In their "photoexcited" states they cause resonant states to occur near zero bias which lead to conductance minima near zero bias with the line shape[7] $\Delta G_2^e(V) \propto |V|$ at zero temperature for small $|V|$. Inelastic tunneling via excitation of a transition (probably electronic) in the photoexcited state is thought[45] to be responsible for the extra current for $V \geq 150$ meV. Thus if the photons cause Δn "Au" complexes to alter their charge state, the photo-induced changes in the total elastic (I^e) and inelastic (I^i) currents are given by

$$\Delta I^e = -(\Delta n) I_1^e(V) + \Delta n I_2^e(V) \ , \tag{6a}$$

$$\Delta I^i = \Delta n I_2^i(V) \ , \tag{6b}$$

in which $I_2^e(V)$ is the normalized resonant-elastic current form factor and $I_2^i(V)$ is the normalized inelastic-current form factor.[45] As $G_2^e = dI_2^e/dV = 0$ at $V=0$, Eqs. (2) predict the linear relation between $-\Delta G^e(V=0)$ and $\Delta I^i(V>150$ meV) shown in Fig. 4. The conductance *decrease* at $V=0$ is attributed to the decrease in the number of complexes in the initial state. In the photoexcited state they cause resonant-elastic tunneling and inelastic tunneling. Both of these effects cause conductance increases for $|V|>0$.

Summarizing, by the use of unique features of the photosensitivity of the tunnel characteristics we eliminated average-barrier tunneling as the major tunneling mechanism in the lightly doped GaAs (Zn : Au-Ge) and argue that the dominant tunneling mechanism is impurity-assisted tunneling (both elastic and inelastic) for these units. We interpret the tunneling at low bias to be a combination of resonant and nonresonant elastic–impurity-assisted–tunneling mechanisms. The large photostimulated peak in the current near 250 meV at forward bias is identified with an inelastic-tunneling process.

C. Bias-Dependent Noise Currents

As might be suspected,[58] the noise generated in a junction is closely connected with the tunneling mechanisms that are operative. For the diodes of this work it can be associated directly with impurity-assisted tunneling. Bias-dependent photosensitive excess-noise currents are detected in lightly doped tunnel diodes only when the Au-Ge impurity is used in the n-type alloy. This impurity in turn leads to noise currents associated with inelastic impurity-assisted tunneling.

In Fig. 5(a) we display both the I-V characteristic and the noise current of a photosensitive diode fabricated on a moderately doped p-type substrate with an n-type alloy containing Au-Ge. Two major points illustrated by this figure are (a) the bias-dependent excess-noise current, and (b) the photosensitivity of the excess-noise current. The existence of this noise current indicates a random populating and depopulating of traps in the barrier as its origin.[59] Furthermore, it is only with the application of sufficient bias that the states responsible for the noise become available for tunneling and to generate noise. The photosensitivity allows us to identify the excess-noise current directly with the Au-Ge–induced inelastic-tunneling mechanism described above.

Studies of the dependence of the excess-noise currents on temperature, substrate doping, and n-type junction alloys have been performed.[60] For diodes leading to results comparable to those shown in Fig. 5(a), we find that at room temperature and 77 °K the excess-noise currents are no longer detectable. We also find that for otherwise similar diodes fabricated on heavily doped p-type substrates

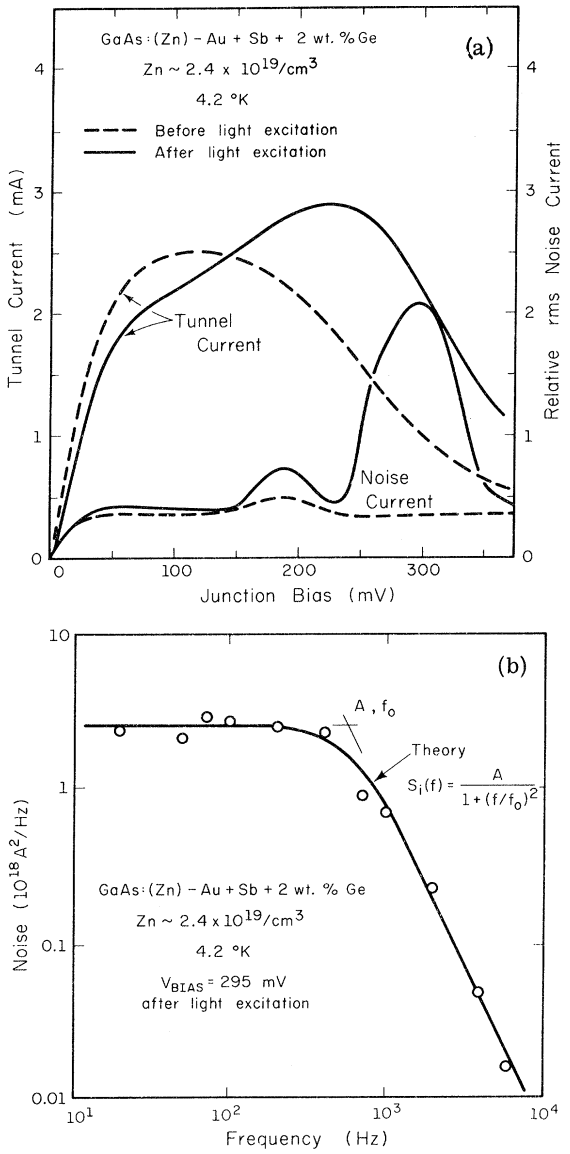

FIG. 5. (a) I-V and rms noise current vs bias at 4.2 °K for a GaAs(Zn:Au-Ge) tunnel diode. The dashed curves are obtained in the dark. The solid curves are obtained after saturation of changes in the characteristics with the radiation output of a tungsten lamp. The background noise has been subtracted out quadratically from the total noise current. (b) Spectral density ($\langle I^2\rangle/\Delta f$) vs frequency of the noise peak at 295 mV in the solid curve of (a). The solid curve is a fit of Eq. (7) to the data.

the noise currents remain bias dependent but are no longer photosensitive. Furthermore, if the n-type alloy system, e.g., Sn or Au-Sn, does not contain Au-Ge impurities, then no appreciable excess-noise currents are detectable for either the lightly or the heavily doped substrates.

Finally, we show in Fig. 5(b) the noise spectrum of the excess-noise current at a bias of 295 mV for the tunnel diode of Fig. 5(a). This noise current can be described by the expression[54]

$$S_i(f)=\frac{A}{1+(2\pi f\tau)^2}\ ,\quad \tau=\frac{1}{2\pi f_0}\ , \tag{7}$$

where $A=3\times10^{-18}$ A^2/Hz and $\tau=0.27$ msec for this particular diode. Such a form of the spectral density is relevant for a noise current which consists of a series of random events with time dependence $i(t)\propto e^{-t/\tau}$, where τ is the decay time of the current fluctuation. This form of time dependence is consistent with a model incorporating real intermediate states of the electron at impurities in the barrier.

D. Correlation of Tunneling Mechanisms with Studies of Au-Ge–Doped GaAs Epitaxial Layers

A central question concerning the results reported in Secs. III A–C concerns their universality. Are they general characteristics of tunneling in III-V semiconductors or peculiar features of p-n tunnel diodes in GaAs (Zn : Au-Ge)? In this section we examine the extent to which these results are peculiar to the alloy-regrowth p-n diode configuration. In particular we study "intrinsic" properties of layers of the GaAs : Au-Ge n-type materials[57] and those of metal contacts on these layers. In particular, for MS contacts on epitaxial layers of GaAs, grown from a melt doped with Au-Ge and saturated with GaAs, we observe photosensitivity in the conductance about zero bias.[9] This allows us to confirm our model of resonant-elastic tunneling via photosensitive states in both MS contacts and tunnel diodes. From luminescence studies we find[57,60] that the recombination processes in these epitaxial layers are dominated by nonradiative recombination through traps in the forbidden gap. The existence of one such trap in these layers is identified by impurity photoconduction, as described below.

As described in Sec. II, to grow the Au-Ge–doped GaAs layers, a melt of Au-Sb eutectic plus a few percent Ge is saturated with GaAs at the growth temperature and is placed in contact with a GaAs substrate. Au-Ge–doped GaAs epitaxial layers are grown during the cool-down cycle. Thicknesses of a few microns to a few mils can be grown depending upon the cool-down cycle and the temperature range employed. Carrier concentrations and mobilities are determined on van der Pauw samples.[61] The measurements yield carrier concentrations of $(4-5)\times10^{18}$ cm^{-3} and Hall mobilities of ~600 cm^2/V sec. These mobilities are relatively low, which is probably due to both doping with Au-Ge and to the amphoteric nature of Ge. We mention that this is the only report of the liquid epitaxial growth of degenerate n-type GaAs doped with Ge.[62]

To correlate the tunneling mechanisms in tunnel diodes (as discussed in Sec. III B) with tunneling in

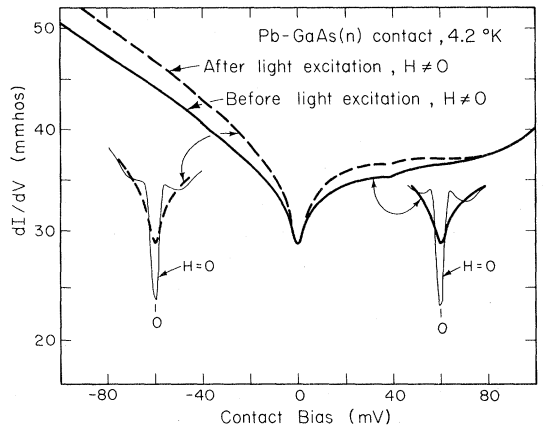

FIG. 6. G-V characteristics at 4.2 °K of Pb contacts on GaAs formed by solution growth of GaAs(Au-Ge) from Au-Sb+2% Ge. The solid curves indiate the characteristics before excitation and the dashed curves those after saturation with the radiation output of a Hg lamp. The insets show the Pb superconducting-gap structure prior to its quenching by a magnetic field [after Duke *et al.*, Ref. 9).

MS contacts, we prepared metal contacts on Au-Ge-doped epitaxial GaAs layers. Both as-grown and etched surfaces of these layers were degassed in high vacuum at 400 °C as a pre-evaporation procedure.[28] The evaporation of a Pb film as the metal contact to the semiconductor was followed by the evaporation of a Au film to serve as a protective coating on the Pb. The conductance characteristics for such a unit are shown in Fig. 6. A satisfactory Pb superconducting energy-gap characteristic, shown in the insets, indicates that an appreciable fraction of the current is due to tunneling. The invariance of $G(V=0)$ to the excitation is evident as is the increase in the apparent "width" of the minimum upon photoexcitation. The gap characteristic appears slightly less satisfactory after the excitation, but the change in the cusp structure near the LO-phonon energy (a "self-energy"-type structure)[27,33–35,63] is not discernible. Therefore the characteristics of the MS contact appear most compatible with a model in which for $|V|>0$ most of the current flows via nonresonant elastic tunneling (perhaps through an average barrier). A small amount of additional resonant (or "two-step") elastic tunneling occurs via trap states in the barrier, as observed by Cullen[13,64] in the context of zero-bias conductance minima in tunnel junctions on p-type silicon. We conclude that the photoexcitation activates trap states near the Fermi energy in both p-n tunnel diodes and MS contacts. The zero-bias conductance minima in these units are associated with resonant ("two-step") tunneling via these states and not with any of the mechanisms to which similar minima have been attributed in the literature.[19–25,62]

To study further the traps in these Au-Ge-doped GaAs epitaxial layers, photoconductive samples were prepared from layers grown on semi-insulating substrates. The response of the photoconductive samples at 77 °K to various wavelengths of radiation is shown in Fig. 7. The most important aspect of these data is that impurity photoconduction occurs for $h\nu < E_g$. It is expected that for a degenerate n-type sample the photoconductive process involves the excitation of an electron from the Au-Ge impurity state to the Fermi level in the conduction band. From Fig. 7 we obtain an excitation energy of (1.36±0.015) eV for the impurity complex and 1.52 eV for the fundamental absorption. From these energies we estimate the position of the impurity state as (160±15) meV above the valence-band edge. This indicates that the same trap occurs in both the grown layers and the p-n tunnel junctions.

Finally, concerning the universality of the observed phenomena, we note that photosensitive effects similar to those shown in Fig. 6 have been observed in GaAs : Zn p-n tunnel diodes in which Sb-Ge rather than Au-Ge is the trap-inducing impurity in the n-type alloy-regrowth region. Although no large increase in the current near 250-mV forward bias was observed, the zero-bias conductance remained constant while the conductance around zero bias increased upon excitation. These results and those described above suggest that whereas the occurrence of the large photosensitive inelastic channel is peculiar to p-n tunnel diodes containing the Au-Ge "impurity" complex, the occurrence of zero-bias conductance minima associated with resonant-elastic tunneling via trap states is a general feature of all types of tunnel

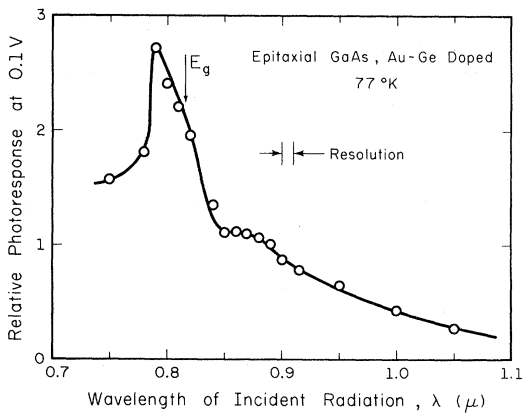

FIG. 7. Photoresponse of a GaAs photoresistor, formed by solution growth of GaAs(Au-Ge) from Au-Sb+2% Ge, to various wavelengths of chopped radiation at 77 °K and 100-mV bias.

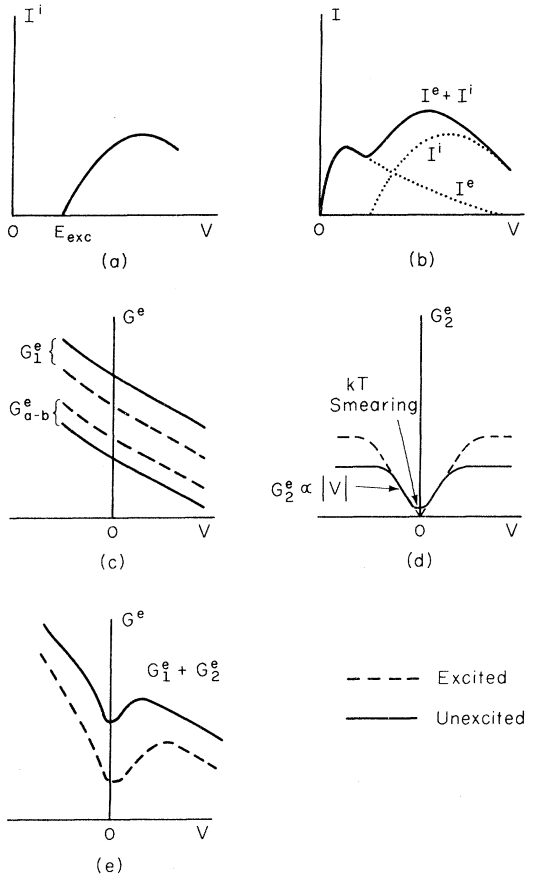

FIG. 8. Qualtative features of the effects upon the I-V and G-V characteristics of various tunneling mechanisms. (a) I-V dependence of the inelastic impurity-assisted tunneling with excitation energy E_{exc}. (b) Total I-V due to elastic and inelastic components of tunneling. (c) G-V curves due to nonresonant elastic (G_1^e) tunneling and tunneling through an average barrier (G_{a-b}^e). The solid curves would be obtained before any excitation and the dashed curves would be expected after excitation. (d) G-V curves due to resonant-elastic (G_2^e) tunneling with and without excitation. (e) Effects upon G-V due to both resonant-elastic and nonresonant-elastic tunneling with and without excitation.

junctions on moderately doped ($p \lesssim 3\times10^{19}$ cm^{-3}) Zn-doped GaAs substrates.

E. Summary of Qualitative Features of I-V and G-V Characteristics and Tunneling Mechanisms

In subsequent sections we utilize the insight about tunneling mechanisms gained in this section and in the literature on phonon-induced tunneling phenomena[1-5,15-18,25,33-35] to infer from the tunneling characteristics qualitative information about the defect structure and local-mode or optical-phonon spectrum of semiconductor tunnel diodes. Our central result is the documentation of a relationship between substrate doping and tunneling mechanisms. We already have seen (Sec. III A) that the one-electron average-barrier model adequately describes only data from heavily doped substrates (the occurrence of dopant-fluctuation phenomena[24,44] notwithstanding). At lower dopings (Secs. II B and D), $p \lesssim 3\times10^{19}$ cm^{-3} for Zn-doped GaAs, (other levels for other dopants and substrates) various types of impurity-assisted tunneling dominate the low-temperature "tunneling" characteristics of semiconductor diodes. The impurity-assisted elastic-tunneling mechanisms and an electronic inelastic mechanism have been described above. Phonon-induced impurity-assisted mechanisms will be described in Sec. V. However, we already have at our disposal enough information to proceed with our qualitative junction-characterization program. As an aid in this program, we review in Fig. 8 those features of the I-V and G-V curves characteristic of the individual and composite tunneling mechanisms required in the interpretation of the data shown in Figs. 2, 4, and 6.

In Fig. 8(a) we illustrate the inelastic–impurity-assisted–tunneling mechanism with an associated excitation energy E_{exc} with $E_{exc} = (150 \pm 10)$ meV for the photosensitive diodes of this work. The total current due to both elastic and inelastic tunneling is shown in Fig. 8(b).

In Fig. 8(c) we compare the impurity-assisted nonresonant and average-barrier elastic currents, where G_1^e describes the former and G_{a-b}^e the latter. We also show the expected changes in the conductances due to photoexcitation. In Fig. 8(d) the resonant-elastic tunneling conductance is shown both before and after excitation. Finally, in Fig. 8(e) we indicate the combined effects of nonresonant– and resonant–impurity-assisted–elastic tunneling upon the conductance both before and after excitation. In constructing this figure we assume the existence of resonant- and nonresonant-elastic channels to be mutually exclusive. If the excitation predominately opens new resonance channels, $G(V=0)$ will be unaffected by the excitation process and the line shapes change as shown in Fig. 6.

Figure 8 provides a convenient "dictionary" of phenomena for our use in Sec. IV to characterize junctions in new ternary mixed-crystal semiconductor compounds.

IV. USE OF TUNNELING TO CHARACTERIZE III-V SEMICONDUCTOR ALLOYS

Having shown that the Au-Ge impurity system in GaAs tunnel diodes introduces states near the Fermi level that give rise to large photosensitive zero-bias conductance minima, we would expect that similar states in the barrier from any other source would produce similar effects. Of particular interest is the possibility that in mixed-crystal systems with lattice mismatch, defects introduced

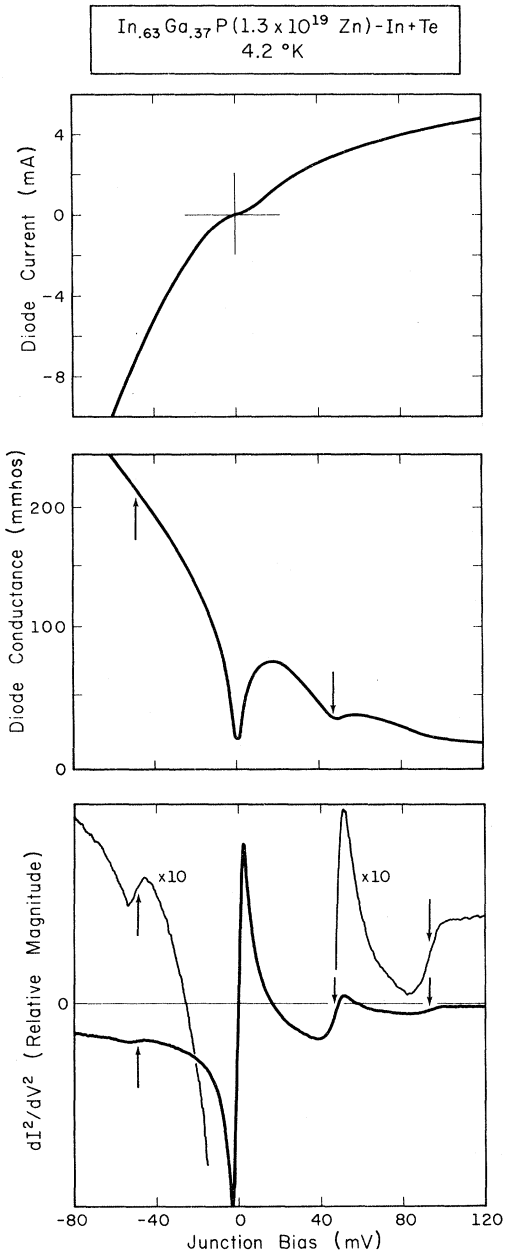

FIG. 9. Tunneling characteristics of an $In_{0.63}Ga_{0.37}P$ (Zn: In-Te) alloyed p-n junction at 4.2 °K showing zero-bias conductance minimum and effects due to optical-phonon interactions (after Korb *et al.*, Ref. 32).

during crystal synthesis or device fabrication because of the mixmatch may cause characteristic manifestations in the tunneling characteristics. The alloys $Ga_{1-x}Al_xAs$,[65,66] $GaAs_{1-x}P_x$,[67-69] and $In_{1-x}Ga_xP$[32,70] are important materials in the construction of electroluminescent devices. Therefore the characterization of the defect structure and its dependence upon synthesis and fabrication conditions is a necessary task. We present in this section data on p-n tunnel junctions in $Ga_{1-x}Al_xAs$, $GaAs_{1-x}P_x$, and $In_{1-x}Ga_xP$ which indicate that transient crystal-growth conditions in a mismatched alloy system introduce a high probability for the formation of defects (improvements in the processing techniques of these materials might reduce the number of defects and the concomitant two-step tunneling).

We also present data that illustrate the influence of phonons on the tunneling electrons and provide information about the lattice vibrational spectra of these alloys. The data confirm earlier optical measurements of the phonon spectra in $Ga_{1-x}Al_xAs$[71] and $GaAs_{1-x}P_x$[72,73] and confirm theoretical predictions of the phonon-mode structure in $In_{1-x}Ga_xP$.[74]

In a preliminary report[32] we showed the tunneling characteristics of an $In_{0.63}Ga_{0.37}P$ p-n junction formed by alloying an In+Te dot on a Zn-doped substrate; those data are reproduced here in Fig. 9 for convenience. The I-V characteristic is that of a backward diode with excess current in the forward direction preventing the appearance of a negative resistance region. The existence of tunneling as the predominant current-flow mechanism is inferred from the temperature independence between 4.2 and 77 °K of the I-V characteristic, except for the fine structure, and from the zero-bias conductance minimum and the LO-phonon fine structure which are observed. Such structure is observed in the diodes described above in Sec. III and in other III-V p-n tunnel diodes in which tunneling is unequivocally indicated by the existence of a negative resistance region.[1,9]

The pronounced zero-bias conductance minimum is attributed to resonant-elastic tunneling through states in the barrier introduced by the formation of structural defects in the crystal.[32] The lattice constants of InP and GaP are approximately[75] 5.869 and[75] 5.451 Å, respectively. With such a degree of lattice mismatch the transient-junction growth process described in Sec. II can be expected to yield badly strained regions and dislocations in the junction, a fact we have been able to confirm directly on liquid-phase-epitaxial (LPE) layers of similar material.[39] These defects produce excess currents in forward bias for $V \geq 100$ mV via impurity-assisted tunneling[76,77] and cause the zero-bias conductance dip as indicated above.

Another factor which appears to affect adversely the crystal quality is a high concentration of Zn impurities. $In_{1-x}Ga_xP$ crystals heavily diffused with Zn are found to have reduced mobilities and when optically excited are extremely weak in photoluminescence.[70] Both observations indicate the presence of a high concentration of nonradiative recombination centers. The details of the defect-producing mechanism are not understood. Because of the

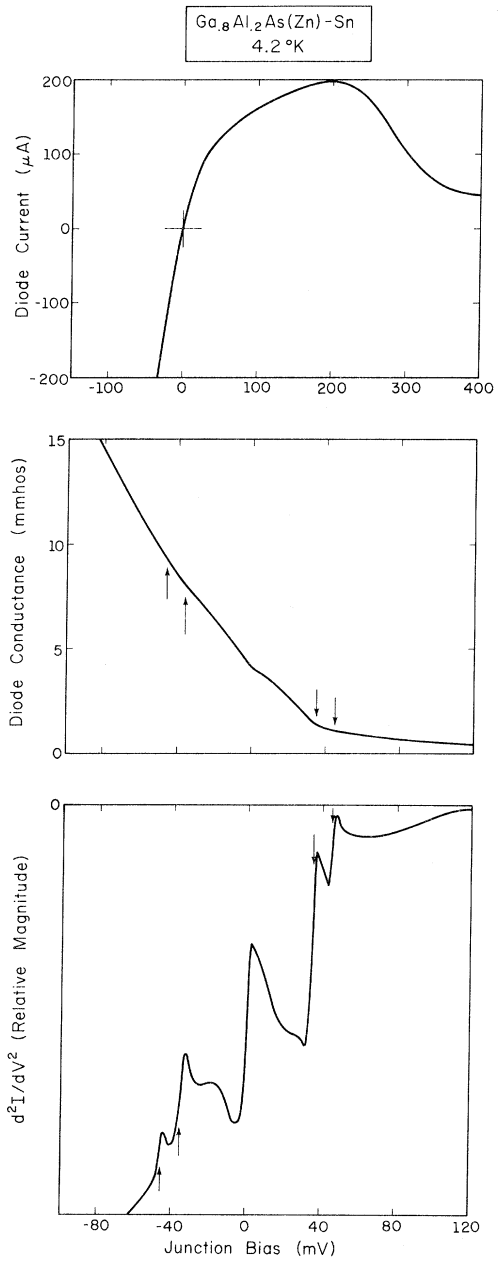

FIG. 10. *I-V*, *dI/dV*, and d^2I/dV^2 characteristics of a $Ga_{0.8}Al_{0.2}As$(Zn:Sn) tunnel diode at 4.2 °K.

large lattice mismatch in $In_{1-x}Ga_xP$, however, it is plausible that the further disorder introduced by substituting Zn in the In-Ga sublattice can give rise to lattice defects. These effects have been minimized in electroluminescent diodes by reducing the Zn concentration,[70] but this is not possible in tunnel junctions because of the necessity of maintaining a high Zn concentration to produce a narrow tunneling barrier. It has not been possible to fabricate $In_{1-x}Ga_xP$ tunnel diodes with negative-resistance regions.

The tunneling characteristics, shown in Fig. 10, of a $Ga_{0.8}Al_{0.2}As$ tunnel diode with a Sn donor dopant contrast sharply with the $In_{0.63}Ga_{0.37}P$ diode characteristics. The *I-V* characteristic in Fig. 10 exhibits a good negative-resistance region with a peak-to-valley ratio of 4.3:1. In addition, the conductance curve is nearly smooth at zero bias, indicating a small amount of resonant-elastic tunneling. The near-perfect lattice match between GaAs (5.653 Å)[75] and AlAs (5.662 Å)[75] permits the fabrication of tunnel diodes with few structural defects caused by lattice mismatch. Correspondingly less tunneling current is stimulated by defect states in the barrier.

The alloy $GaAs_{1-x}P_x$ presents an example of a system with an "intermediate" lattice mismatch (GaP: 5.451 Å)[75] in which the effects of defect formation during junction regrowth are less severe than in $In_{1-x}Ga_xP$ but yet are quite noticeable. Tunneling characteristics of a $GaAs_{0.5}P_{0.5}$ diode made using a Sn + Te alloy are shown in Fig. 11. As with the $In_{0.63}Ga_{0.37}P$ diode shown in Fig. 9, excess current at forward bias >100 mV prevents a negative-resistance region from appearing in the *I-V* characteristic. The highest *P* content that allowed fabrication of a diode with a negative resistance region was $x = 0.45$.

The modest magnitude of the conductance dip at zero bias indicates the diminished importance of resonant-elastic tunneling relative to that observed in $In_{1-x}Ga_xP$. This appears to result from the better lattice match as well as the fact that the substrate doping does not disturb the sublattice of varying composition.

The difficulty which we experienced in making alloyed *p-n* tunnel diodes in $In_{1-x}Ga_xP$ and $GaAs_{1-x}P_x$ corresponds to other problems encountered in making devices in mismatched alloy systems. For example, Alfëov *et al.*[78] and Craford *et al.*[79] observed high densities of nonradiative recombination centers in $GaAs/GaAs_{1-x}P_x$ heterojunctions which adversely affect luminescent properties of the junctions. In the work presented here, the rapidly changing junction-growth conditions cause a sharp compositional change in the *n*-type side of the junction. This fact has the consequence that the lattice mismatch becomes a source of high defect density.

The data in Figs. 9–11 indicate that tunneling provides a means for studying the lattice vibrational spectra of mixed crystals. The phonon line shape in Fig. 9 at 44.6 meV shows the existence of a single optical-phonon mode in this diode. As previously reported,[32] this single-mode behavior persists in $In_{1-x}Ga_xP$ for the complete composition range $0 \leq x \leq 1$, as shown in Fig. 12. The phonon energy varys nearly linearly with composition from 42.5 meV in InP to 49.5 meV in GaP. This observation

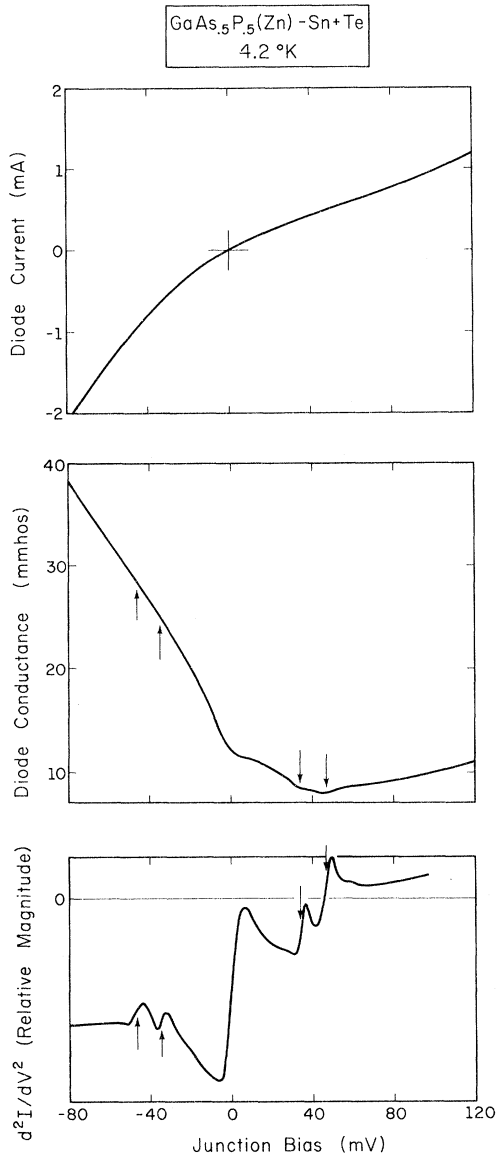

FIG. 11. I-V, dI/dV, and d^2I/dV^2 characteristics of a $GaAs_{0.5}P_{0.5}$(Zn:Sn-Te) tunnel junction at 4.2 °K.

confirms the prediction of Lucovsky *et al.*[74] based on their calculation of local-mode frequencies of dilute impurities in crystals, that $In_{1-x}Ga_xP$ should have a single observable optical-phonon mode near $\vec{k}=0$.

The LO-phonon-mode structure in $Ga_{0.8}Al_{0.2}As$ is more complicated, as is evident from the d^2I/dV^2 characteristic in Fig. 10. The higher-energy mode at 45 meV becomes steadily more pronounced as the Al content is increased. Two-mode behavior is observed by Ilegems and Pearson[71] in optical experiments over the compositional range for $0.08 \leq x \leq 0.82$ and in this work for $0.03 \leq x \leq 0.20$. The dependence upon x of the energies of the two modes near $\vec{k}=0$ is shown in Fig. 12. These data are in reasonable agreement with the optical data mentioned above[71] and with predictions of Chang and Mitra[80,81] based on a "modified random-element isodisplacement" model. The model predicts the existence of the two modes and gives the composition dependence of the optical-phonon-mode frequencies.

Similar behavior of the LO-phonon modes near $\vec{k}=0$ is observed in $GaAs_{1-x}P_x$, with two modes easily seen in the d^2I/dV^2 curve in Fig. 11. As expected, the strength of the higher-energy mode increases with increasing P content. The composi-

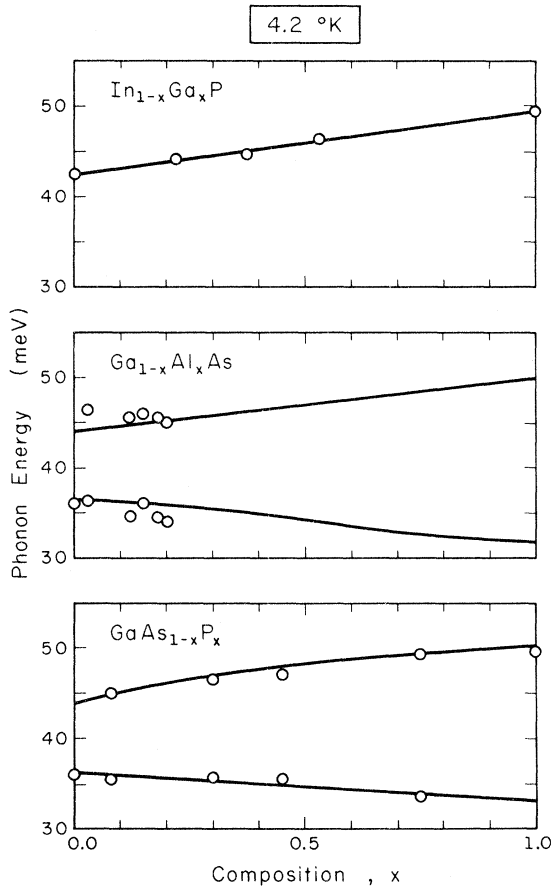

FIG. 12. Top panel: optical-phonon energies in $In_{1-x}Ga_xP$ as a function of composition x, showing single-mode behavior. The line is a linear fit to the data. Center panel: optical-phonon energies in $Ga_{1-x}Al_xAs$ as a function of composition x, showing the existence of two LO-phonon m modes. The lines follow the prediction of Chang and Mitral (Ref. 80). Lower Panel: optical-phonon energies in $GaAs_{1-x}P_x$ as a function of composition x. Two-mode behavior is evident for all x. The energy dependence of the upper mode drawn is calculated by Verleur and Barker (Ref. 72). The line through the low-mode data is a linear fit.

tional dependence of the phonon energies is shown in Fig. 12 and is in agreement with data from reflectivity[72,73] and transmittance[73] measurements of the number and energy of LO-phonon modes near $\vec{k}=0$. A number of computational models satisfactorily explain the observed spectra.[72,73,81]

We mention that all experimental phonon energies were corrected for series resistance in the diodes. The energies are identified with bias values at points of maximum slope in the d^2I/dV^2 curves, corresponding to the center of cusplike structures in the conductance associated with electronic-self-energy effects[33-35] as corrected for strong polar coupling.[82] Duke and co-workers have predicted the dI/dV and d^2I/dV^2 line shapes expected due to both bulk[33-35] and local-mode[17,18,36] electron-phonon coupling in MS contacts. In the case of deformation-potential coupling to optical phonons in Si:B, both the calculated[33-35] and observed[1,10] structures in heavily doped units are cusplike features in dI/dV at $eV \simeq \pm\hbar\omega_{LO}$ which are antisymmetric about zero bias. The structures observed in our diodes are similar except that they are symmetric about zero bias. This symmetry is characteristic of all the p-n tunnel diodes which we have examined. It suggests the predominance of unscreened polar coupling of the electrons to impurities in the space-charge region.[33,35,82] Similar structure is observed in metal contacts on p-type GaAs[28] and lightly doped[10,59] Si:B as well as in GaAs p-n tunnel diodes.[9]

The existence of one- or two-phonon modes in mixed crystals is thought to be dictated by the impurity-mode behavior in the crystal in the limits $x=0$ or 1.[83] Specifically, in order for two-mode behavior to appear over the compositional range, in the limit of low concentration ($x \to 0$ in $Ga_{1-x}Al_xAs$ and $GaAs_{1-x}P_x$) the light constituent must have a local vibration mode above the optical-phonon band in the host crystal. In the $x \to 1$ limit, the heavy constituent must give rise to a gap mode in the light host crystal.[83] These conditions are satisfied in $Ga_{1-x}Al_xAs$ and $GaAs_{1-x}P_x$, and two-mode behavior is observed. Neither condition, however, is satisfied in $In_{1-x}Ga_xP$, and single-mode behavior is observed over the complete compositional range.

A general observation concerning the phonon line shapes is the increasing sharpness of the line shape as the lattice match improves from $In_{1-x}Ga_xP$ to $GaAs_{1-x}P_x$ to $Ga_{1-x}Al_xAs$. While it is difficult to describe this trend quantitatively, the suggestion that clustering of like atoms in a mismatched system tends to occur[72] would explain some amount of broadening through local compositional inhomogeneity. Such clustering inevitably occurs for some ternary crystals (e.g., $GaAs_{1-x}P_x$ or $In_{1-x}Ga_xP$) during the alloying of the junction even if the substrate does not exhibit any inhomogeneity.[73]

Summarizing, the important points of this discussion are that transient growth conditions in mismatched III-V semiconductor alloys (and presumably other crystal systems) introduce a high probability for the creation of crystal defects, and that these defects are detectable in tunneling experiments. Such transient conditions are present during the preparation of alloyed tunnel diodes and during LPE growth of crystal layers in a cool-down growth cycle.[39,84] We have presented data showing that resonant-elastic tunneling occurs through such defect states and gives rise to pronounced zero-bias conductance minima. The tunneling data also yield information on the number and energies of the $\vec{k}=0$ LO-phonon modes in the III-V alloys studied. Thus we conclude that tunneling provides a useful technique for the characterization and study of these mixed-crystal systems.

V. IMPURITY-ASSISTED TUNNELING: THEORY

In previous sections we both documented the dominance of resonant-impurity-assisted-tunneling processes in junctions on "moderately" doped substrates and utilized their qualitative manifestations to characterize junctions in III-V mixed-crystal alloys. Having demonstrated the importance of these processes in laboratory semiconductor diodes, we investigate three questions. What is the relationship between the microscopic concept of resonant-elastic tunneling[36,55] and the kinetic concept of "two-step" tunneling?[6-8] Given that resonant-tunneling processes are important in the elastic tunneling channels, what are their concomitant consequences in the inelastic channels?. Finally, and perhaps of most importance, to what extent can the observed manifestations of resonant-tunneling phenomena be used to characterize the position, electronic, and vibronic structure of the defect which is responsible for the resonance?

In this section we develop insight into these questions by analyzing the model of a vibrating δ-potential impurity within the context of a new theory of tunneling[17,18,85] which, unlike the transfer-Hamiltonian theory,[1] simultaneously describes both resonant and inelastic phenomena. In Sec. V A we review the final expression for the current predicted by the theory for this model. The model's description of zero-bias conductance minima by means of resonant-elastic tunneling is outlined in Sec. V B, as is the relation between microscopic "resonant-elastic" tunneling and kinetic "two-step" tunneling. In Sec. V C we note the features of nonresonant-inelastic tunneling and their (satisfactory) comparison with experimental data characterizing units on heavily doped substrates. Our major results are presented in Sec. V D: the derivation of the relation between resonant-elastic and resonant-inelastic tunneling and the documentation that the manifestations of this relation are evident in the tunnel char-

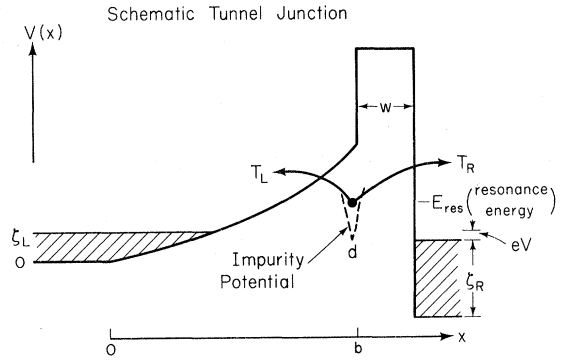

FIG. 13. Schematic M-O-S junction with an attractive impurity potential $U(x)$. In the text, $U(x)=U_0\delta(x-d)$, so that the impurity potential is completely localized at $x=d$. $T_L(T_R)$ is the probability for transmission of an electron from the impurity site to the left (right) electrode. In the drawing, $T_L \simeq T_R$, so that the impurity potential is resonant.

acteristics of a wide variety of semiconductor diodes, including some of those described above in Secs. III and IV.

A. Predictions of Extended-Basis-Function Theory

The essential theoretical difficulty with which the data presented in Secs. III and V confront us is simply stated: No single theory of tunneling developed to date is adequate to describe both resonant tunneling and inelastic tunneling. One-electron average-barrier models have been employed for years to give qualitative descriptions of resonant-elastic-tunneling processes.[1,36,86] Similarily, the transfer-Hamiltonian method, in both its momentum-representation[1,25] and configuration-representation[35,87] versions, has been applied to describe phonon effects in tunneling. The latter method cannot adequately describe resonance effects due to its use of the tunneling probability as a (small) expansion parameter.[1,18] The former method has been extended to include phonon-assisted tunneling via coupled-channel analyses.[15,16,88] However, no explicit consideration of resonance processes has been given using the multichannel-scattering-theory methods. They also exhibit certain difficulties in treating the Pauli exclusion-principle restrictions on the electrons in a consistent fashion.[18] The results presented below are based on the extended-basis-function method of evaluating tunneling currents[17,18,85] in which current-carrying eigenstates of the entire junction are used as basis states for a perturbation-theory analysis of electron-impurity, electron-phonon, and electron-electron interactions. The consequences of all of these interactions first are evaluated for an equilibrium system (i.e., at zero bias) using conventional techniques.[89] Then, the nonequilibrium current induced by a finite bias is evaluated by using the analytic continuation technique proposed by Kleiman and Duke.[18,85] The predictions of the transfer-Hamiltonian method[1,25,35,87] can be recovered by appropriate expansions of the extended-basis-function results.[18]

For our purposes here, we merely examine the form of the extended-basis-function predictions for a model of static δ-function impurities, $U(\vec{r}-\vec{R}) = -U_0\delta(\vec{r}-\vec{R})$, vibrating at a given local-mode frequency ω_0, i.e.,

$$\vec{R}(t)=\vec{R}(0)+\vec{u}\cos\omega_0 t\ ,$$

of the impurities. We further consider the impurities to be periodically arrayed in a plane located at $x=d$ parallel to the junction and the impurities are allowed to vibrate with frequency ω_0 only in the x direction. The spatial and energy conventions are illustrated in Fig. 13. The current resulting from this model is given, in the weak-electron-phonon-coupling limit, by the following expression[18,85]:

$$J(eV)\cong\frac{2e}{h}\int_0^\infty dE\,[f(E)-f(E+eV)]\int\frac{d^2k_\parallel}{(2\pi)^2}\,|S_{12}(E,\vec{k}_\parallel)|^2 \times[1+2G_1(E,\vec{k}_\parallel)\Sigma_L(E)-G_2(E,\vec{k}_\parallel)\Sigma_2(E)]\ , \tag{8a}$$

$$f(E)\equiv(1+e^{\beta(E-\zeta_L)})^{-1}\ , \tag{8b}$$

$$\beta=\kappa T\ . \tag{8c}$$

In Eqs. (8a) and (8b), E is the total energy of the tunneling electron, we have assumed $\vec{k}_\parallel$ conservation (i.e., neglected umklapp from the impurities), κ is Boltzmann's constant, T is the temperature, and ζ_L is the Fermi degeneracy of the left electrode, as illustrated in Fig. 13. Also, $|S_{12}|^2$ is the barrier-penetration probability, and the quantities G_1 and G_2 (Σ_1 and Σ_2) are the real and imaginary parts, respectively, of the retarded one-electron coordinate-space Green's function (self-energy) evaluated at the position of the plane of impurities. Both the Green's functions and self-energies are sums of two terms representing the contributions from the basis states that carry current from left to right and vice versa:

$$G_0^R(d,d,\vec{k}_\parallel,E)\equiv\int_0^\infty d\epsilon\,\frac{|\psi_L(\epsilon,\vec{k}_\parallel,d)|^2}{E-\epsilon+i\delta} +\int_{\zeta_L-eV-\zeta_R}^\infty d\epsilon\,\frac{|\psi_R(\epsilon,\vec{k}_\parallel,d)|^2}{E-\epsilon+i\delta}\ , \tag{9}$$

$$\Sigma(E)=\Sigma_L(E)+\Sigma_R(E)\ , \tag{10a}$$

$$\Sigma_L(E)\equiv\Lambda_{00}\int_0^\infty d\epsilon\int\frac{d^2k_\parallel}{(2\pi)^2}\,|\psi_L(\epsilon,\vec{k}_\parallel,d)|^2 \times\left(\frac{f(\epsilon)+N(\hbar\omega_0)}{E-\epsilon+\hbar\omega_0+i\delta}-\frac{f(\epsilon)+N(-\hbar\omega_0)}{E-\epsilon-\hbar\omega_0+i\delta}\right), \tag{10b}$$

$$\Sigma_R(E) \equiv \Lambda_{00} \int_{\zeta_L - \zeta_R - eV}^{\infty} d\epsilon \int \frac{d^2 k_{\parallel}}{(2\pi)^2} \left| \psi_R(\epsilon, \vec{k}_{\parallel}, d) \right|^2 \times \left(\frac{f(\epsilon + eV) + N(\hbar\omega_0)}{E - \epsilon + \hbar\omega_0 + i\delta} - \frac{f(\epsilon + eV) + N(-\hbar\omega_0)}{E - \epsilon - \hbar\omega_0 + i\delta} \right) , \tag{10c}$$

$$N(x) \equiv (e^{\beta x} - 1)^{-1} , \tag{11}$$

$$\Lambda_{00} = \gamma^2 N_0^2 p_c \hbar\Omega / 2\pi M \omega_0 . \tag{12}$$

As illustrated in Fig. 13, ζ_R is the Fermi degeneracy of the right electrode. The quantities ψ_L and ψ_R are, respectively, the left and right current-carrying extended-basis functions[90] of total energy ϵ and parallel momentum $\vec{k}_{\parallel}$, which are evaluated at $x = d$. These wave functions are normalized to a δ function in energy[91] and are mutually orthogonal.[92] The quantity Λ_{00} is a coupling constant in which γ is the strength of the vibrating δ function, R_0 is the number of vibrating impurities per unit area, p_c is the cutoff momentum for phonons propagating in the x direction, Ω is the volume of a primitive cell in the host crystal, and M is the mass of an ion.

Upon examining the expression for the current in Eq. (8a), we see that the first term in square brackets gives rise to the ordinary one-electron tunneling current. The terms which involve Σ_1 and Σ_2, are, respectively, the reactive and dissipative contributions to the current. They have been assumed to be small relative to unity in deriving Eq. (8a) so that a denominator could be expanded.[18] We now turn to an examination of these terms individually.

B. Relation between Zero-Bias Anomalies and Resonant-Elastic Tunneling

In this section, we examine the effect of resonant-impurity potentials upon the one-electron tunneling current. The condition that an attractive potential in the barrier of a tunnel junctions at $x = d$ produces a resonance in the barrier-penetration probability $|S_{12}|^2$ is that T_L, the tunneling probability from the impurity site to the left electrode, must equal T_R, the corresponding probability of tunneling to the right electrode, as illustrated in Fig. 13. In the WKB limit, the barrier-penetration probability is approximately given by[18,85]

$$|S_{12}|^2 \cong |S_{12}^0|^2 \left(1 + \frac{4[V(d) - E_r]^2}{(E_\perp - E_r)^2 + \gamma_{\mathrm{WKB}}^2} \right) , \tag{13a}$$

$$|S_{12}^0|^2 \cong (v_R / v_L) T_L T_R , \tag{13b}$$

$$E_\perp \equiv E - \hbar^2 k_{\parallel}^2 / 2m , \tag{14}$$

$$\gamma_{\mathrm{WKB}}^2 \equiv (2\hbar^2/m)[V(d) - E_r] \Gamma_{\mathrm{WKB}}^2 , \tag{15a}$$

$$\Gamma_{\mathrm{WKB}}^2 = \tfrac{1}{4} K_0^2 [(T_L/T_R)^{1/2} + (T_R/T_L)^{1/2}] T_L T_R , \tag{15b}$$

$$K_0 \equiv -mU_0/\hbar^2 , \tag{16}$$

$$E_r \equiv V(d) - U_0^2 m / 2\hbar^2 . \tag{17}$$

The quantities v_R and v_L are the velocities of particles in the right and left electrodes, respectively, and $V(d)$ is the value of the average-barrier potential at the position of the δ-potential impurity.

In order to simplify the calculation of the resonant-elastic current characteristics, we note that for a sharp resonance,

$$\frac{\gamma_{\mathrm{WKB}}}{(E_\perp - E_r)^2 + \gamma_{\mathrm{WKB}}^2} \cong \pi \delta(E_\perp - E_r) . \tag{18}$$

The approximation in Eq. (18) allows us to determine the qualitative effects of resonances upon the tunneling characteristics. Inserting Eqs. (13a), (13b), and (18) into Eq. (8a) yields an expression for the elastic current in which it is written as the sum of a background term J_0 and a resonant term J_r:

$$J(eV) = J_0(eV) + J_r(eV) , \tag{19a}$$

$$J_0(eV) \equiv \frac{me}{2\pi^2\hbar^3} \int_{\zeta_L - eV}^{\zeta_L} dE \int_0^E dE_\perp \left| S_{12}^0 \right|^2 , \tag{19b}$$

$$J_r(eV) \equiv \frac{e}{h} \int_{\zeta_L - eV}^{\zeta_L} dE \frac{K_0^3}{\Gamma_{\mathrm{WKB}}} \left| S_{12}^0(E_r) \right|^2 \theta(E_r)\, \theta(E - E_r) , \tag{19c}$$

$$\theta(x) = \begin{cases} 1 , & x > 0 \\ 0 , & x < 0 \end{cases} . \tag{19d}$$

Two features of Eqs. (19) are important. First, the resonance contribution to the current occurs if the resonance energy $E_r(eV)$ lies in a certain energy range. The second important feature of Eqs. (19) is their prediction that the bias dependence of $E_r(eV)$ and of the integration limits dominate the behavior of $J_r(eV)$ and its derivative $G_r \equiv d(J_r)/d(eV)$. In displaying the consequences of these limits, we find it convenient to regard $R = d(E_r)/d(eV)$ as an independent parameter describing the motion of the resonance state with bias. For this purpose we write

$$E_r = E_0 + ReV , \quad 0 \geq R \geq -1 \tag{20a}$$

$$E_0 = \zeta_L - \Delta , \tag{20b}$$

where E_0 is the position of the resonance energy at zero bias with respect to the bottom of the left electrode's band (the semiconductor in a MS contact and the n-side in a p-n tunnel diode).

The elastic conductance which results from employing Eqs. (19) and (20) are illustrated schematically in Figs. 14 and 15. The zero-bias anomalies (ZBA) in the conductance $G \equiv dJ/d(eV)$ which occur in resonant-elastic tunneling are shown for the cases that $R = -\frac{1}{2}$, and $R = 0$, -1, respectively. We can interpret these structures by examining Eq. (19c). The step function indicates that current flows in the resonant-elastic channel when either $\zeta_L \geq E_r \geq \zeta_L - eV$ (forward bias, in the convention of Fig. 13) or $\zeta_L - eV > E_r > \zeta_L$ (reverse bias). This thresh-

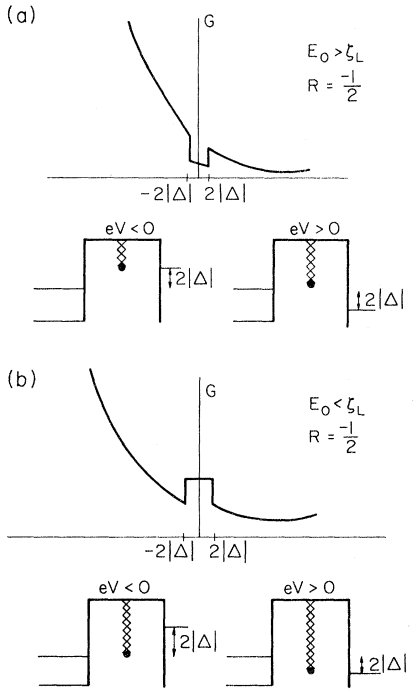

FIG. 14. Resonant-elastic conductance schematically illustrated for $R \equiv dE_r/d(eV) = -\frac{1}{2}$ (i.e., E_r is the resonance energy). E_0 is the resonance energy at zero bias (i.e., $E_r = E_0 + ReV$) and $\Delta \equiv \zeta_L - E_0$ in the conventions of Fig. 13. In (a), $E_0 > \zeta_L$ and in (b), $E_0 < \zeta_L$. Therefore, the resonant-elastic channel opens in (a) [closes in (b)] when $|eV| > 2|\Delta|$. The schematic tunnel junctions in the figure illustrate the switch concept. The black dot represents the resonance energy and the cross hatching indicates the range of energies for which resonant tunneling can occur (after Kleiman, Ref. 18).

old behavior may be regarded as a "switch effect": The resonance is an extra tunneling channel, or "window" in the barrier, since $|S_{12}|^2 \approx 1$ when $E_\perp \approx E_r$. Therefore, tunneling electrons with total energy $E > E_r$ will always be able to see the window (since $0 \leq E_\perp \leq E$). The resonance acts like a "switch": When one of the Fermi levels passes above the resonance, electrons in states with $E > E_r$ are able to tunnel through the resonance, and the resonant-elastic channel is opened. If, at zero bias, the resonance energy is above the Fermi level ($\Delta < 0$), resonant-elastic tunneling appears only when either the right or left Fermi levels pass above the resonance energy. In this case, the conductance exhibits a minimum near zero bias. If, on the other hand, $\Delta > 0$, resonant-elastic tunneling occurs at zero bias. However, when either the right or left Fermi level passes below the resonance energy the resonant-elastic channel is closed for additional electrons to tunnel through. In this case, the conductance exhibits a maximum near zero bias. We conclude that, if $R = 0$ (i.e., the resonance moves in bias with the left Fermi level) and $\Delta < 0$, resonant-elastic tunneling occurs only in reverse bias. The threshold for this process is $eV = \Delta$. By an analogous argument, for $R = -1$ (i.e., the resonance energy moves with the right Fermi level) and $\Delta < 0$, resonant-elastic tunneling occurs only in forward bias with a threshold $eV = -\Delta$. A complete set of results for $R = 0$, -1 and both signs of Δ is given in Fig. 15.

Figures 14 and 15 provide a conceptual framework for interpreting a wide variety of threshold (especially "zero-bias") phenomena.[1] For example, the simple cusp structure shown in Fig. 8(d), i.e., $G^{res} \propto |V|$, results from a uniform distribution in energy of states with $R \cong -\frac{1}{2}$ and $\Delta \leq 0$. Several empirical models have been used to predict such distributions in metal-insulator-metal junctions.[1,6,7,81] Similarily, as we see from Eqs. (13), (15), and (19) that for sharp resonances, $(J_r\hbar/\zeta_L e) \sim (J_0\hbar/\zeta_L e)^{1/2}$, resonance states with $0.3 \lesssim -\Delta \lesssim 0.5$ eV and $R \simeq 0$ provide a microscopic alternative to Parker and Mead's kinetic-theory interpretation of their data.[8] Furthermore, we see from Fig. 13 that some qualitative information about the position in the junction of the resonant-trap state can be in-

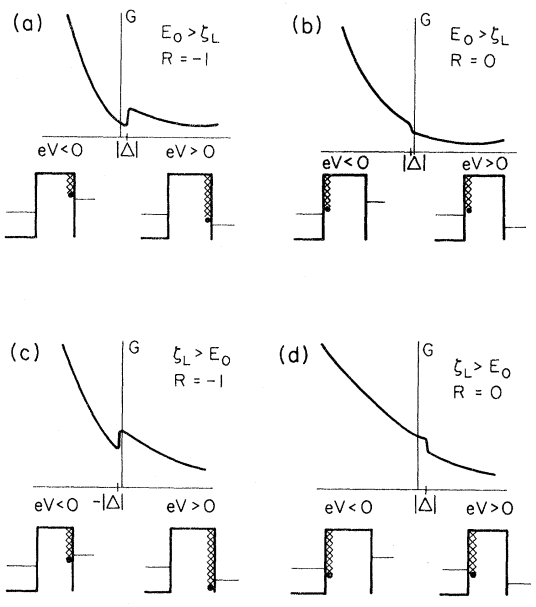

FIG. 15. Schematic illustration of the resonant-elastic conductance as a function of $R \equiv dE_r/d(eV)$ (i.e., E_r is the resonance energy of the impurity potential). E_0 is the resonance energy at zero bias (i.e., $E_r = E_0 + ReV$) and $\Delta \equiv \zeta_L - E_0$ in the conventions of Fig. 13. In (a) and (c), $R = -1$ [i.e., the resonance energy moves with the right (metal) Fermi level]. The resonant-elastic channel opens when either Fermi level passes above the resonance energy. In (a) and (c), the resonant-elastic channel is open only in forward bias, while in (b) and (d), it is open only in reverse bias (after Kleiman, Ref. 18).

ferred from the value of R extracted from the data. Thus for the rather symmetric zero-bias conductance minima which occur in some of our units the trap states occur near the "electronic" center of a junction defined by $d[V(d_0)]/d(eV) \simeq -\frac{1}{2}$. (This would be the geometrical center for only a square-barrier junction.) Similarly, in the case of Parker and Mead's metal contacts on CdTe, we infer that the trap states lie near the edge of the space-charge region in the CdTe. Finally, it seems possible that some of our units and many of those reported on in the literature[10,11,19–24,28–30] are characterized by $|\Delta| \simeq 0$, $R \simeq -1$; i.e., trap states near the metal electrode in MS contacts and metal-insulator-semiconductor junctions and near the edge of the p-type space-charge region in p-n tunnel diodes. Obviously, in all real junctions the distributions in both positions and energy of the trap states smear out the ideal characteristics noted in Figs. 14 and 15.

C. Nonresonant Inelastic Tunneling

As described by Davis and Duke,[33] the nonresonant impurity-mediated contributions to the electronic self-energy, given by Eqs. (10), do not differ in form from those due to electron-phonon interactions in the bulk electrode. A calculation of the nonresonant phonon-induced contributions to the conductance in the case of our δ-potential-impurity model also has been given by Davis[16] using a coupled-channel method. The results obtained from Eqs. (8)–(20) are similar to his in form, but not identical in detail.[18]

In Eqs. (10), the nonresonant impurity-assisted contribution to the self-energy, Σ^{nr}, occurs when the spectral densities $|\psi_\alpha(\epsilon, \vec{k}_{||}, d)|^2$ of the basis states at the impurity position exhibit no sharp maxima associated with quasibound "trap" states on the impurities. In this case we deduce the voltage dependence of the conductance directly from the analytic structure of Σ^{nr} as described, in some detail, by Davis and Duke.[33] We find that $\mathrm{Re}\Sigma^{nr}$ exhibits logarithmic divergence (cusps) and $\mathrm{Im}\Sigma^{nr}$ exhibits steps. These cusps and steps correspond to thresholds for emission or absorption of a phonon by an electron. Such threshold structure occurs at $E = \zeta_L \pm \hbar\omega_0$ in Σ_L^{nr} and $E = \zeta_L - eV \pm \hbar\omega_0$ in Σ_R^{nr}. Therefore we regard the phonon thresholds in Σ_L^{nr} and Σ_R^{nr} as rigidly attached to the left and right Fermi levels, respectively. We consider the self-energies for three different impurity positions: (i) $d = 0$ (i.e., the impurity is near the left (semiconductor) electrode), for which $\Sigma_L^{nr} \gg \Sigma_R^{nr}$; (ii) $d = \frac{1}{2}b$ (i.e., the impurity is midway between the electrodes), for which

$$\mathrm{Re}(\Sigma_L^{nr}(\zeta_L - eV)) \simeq -\mathrm{Re}(\Sigma_R^{nr}(\zeta_L)) ;$$

(iii) $d = b$ [i.e., the impurity is near the right (metal) electrode], for which $\Sigma_R^{nr} \gg \Sigma_L^{nr}$.

Applying the idea that the left and right nonresonant self-energies move rigidly with the left and right Fermi levels, respectively, we draw the simple picture shown in Fig. 16 which describes the effect of the self-energies upon the conductance. When $d = 0$, $\Sigma_L^{nr} \gg \Sigma_R^{nr}$ so the self-energy contribution from Σ_L^{nr} dominates. In this case, we obtain the line shape in Fig. 16(a), i.e., the upward (downward) cusp in reverse (forward) bias in the incremental conductance involving Σ_1^{nr}. We designate this incremental conductance by the symbol G_1^{nr}. The incremental conductance deriving from the current contribution involving Σ_2^{nr} we denote by G_2^{nr}.

If $d = b$, $\Sigma_R^{nr} \gg \Sigma_L^{nr}$, so that the contribution from Σ_R^{nr} dominates. We see a downward cusp in reverse bias and an upward one in forward bias, as in the schematic line shape for G_1^{nr} in Fig. 16(c).

In the intermediate case, $d = \frac{1}{2}b$,

$$|\Sigma_L^{nr}(\zeta_L - eV)| \simeq |\Sigma_R^{nr}(\zeta_L)| .$$

Therefore, the logarithmic cusps in $\mathrm{Re}(\Sigma_L^{nr})$ and $\mathrm{Re}(\Sigma_R^{nr})$ approximately cancel one another. This cancellation has the effect that little or no structure appears in G_1^{nr}, as shown in Fig. 16(b).

Typical experimental conductance line shapes measured in metal-oxide highly degenerate semiconductor junctions [e.g., $Si/SiO_2/Pb(In)$ junctions

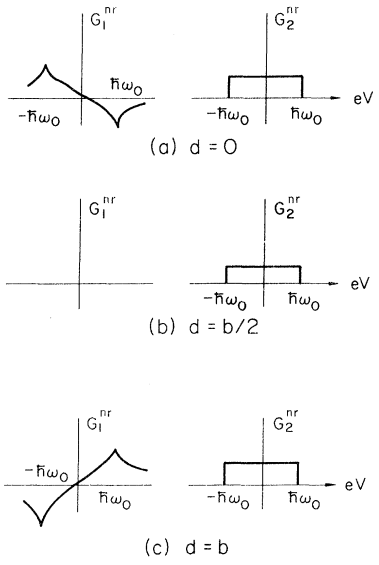

FIG. 16. Schematic dependence of the incremental conductance on the position of a nonresonant impurity potential. (a) $d = 0$ (i.e., the impurity is near the left electrode in the schematic tunnel junction of Fig. 13); $\Sigma_L^{nr} \gg \Sigma_R^{nr}$. (b) $d = \frac{1}{2}b$; thus, $|\mathrm{Re}\Sigma_L^{nr}| \approx |\mathrm{Re}\Sigma_R^{nr}|$ and the contributions from the real parts of the left and right self-energies cancel in G_1^{nr}. (c) $d = b$; $\Sigma_R^{nr} \gg \Sigma_L^{nr}$; due to the symmetric structure in $\mathrm{Im}\Sigma$, G_2^{nr} exhibits the same structure in Figs. 15(a)–(c) (after Kleiman, Ref. 18).

with $N_D \simeq 10^{20}$ cm^{-3} [10,64] exhibit characteristic upward cusps in forward bias and downward cusps in reverse bias which are approximately equal in size. However, from the analysis outlined above we see that the symmetry of the phonon-induced fine structure in the conductance depends upon the impurity's position. An impurity which is near the left (semiconductor) electrode in an MS contact produces phonon line shapes predicted by Davis and Duke[33]; i.e., the phonon structure takes the form of a cusp up (down) in reverse (forward) bias when we choose the voltage conventions illustrated in Fig. 14. If, on the other hand, an impurity is near the right (metal) electrode, the symmetry of the phonon lineshapes is reversed; i.e., a cusp down (up) in reverse (forward) bias.

Most experimental line shapes[10,11,19-24] display phonon line shapes which are much larger in forward than in reverse bias. This asymmetry usually is associated with zero-bias anomalies. Consequently, these line shapes do not exhibit the features predicted by the nonresonant impurity model. In order to explore one mechanism which can cause such asymmetries, we examine the effect upon the current characteristics of the assumption that the impurity ion's potential produces a resonance in the transmission.

D. Resonant–Impurity-Assisted–Inelastic Tunneling

The contribution to the current from resonant-inelastic tunneling [i.e., the last two terms in Eq. (8a)] contains the product of $|S_{12}|^2$ and the self-energy defined in Eqs. (10). Both the barrier-penetration factor, $|S_{12}|^2$ approximately given by Eqs. (13), and the intermediate-state extended-basis functions in the self-energy contain resonant denominators. The resonance in the self-energy has the consequence that only electrons of total energy $E > E_r \pm \hbar\omega_0$, where ω_0 is the phonon frequency, exhibit appreciable probability of inelastically emitting or absorbing a phonon. Therefore, the total contribution from resonant-inelastic tunneling to the current contains both the elastic resonance in $|S_{12}|^2$ and the inelastic resonances in $\Sigma^{\rm res}$, the resonant self-energy. Therefore the resonant-inelastic contribution to the current (and conductance) in Eq. (8a) exhibits phonon-induced fine structure only in those signs of the bias in which the resonant-elastic channel already is open; i.e., asymmetries in the phonon line shapes are accompanied by zero-bias anomalies.

When a δ-function-impurity potential is inserted inside the barrier, as shown in Fig. 14, the absolute value of the extended-basis functions satisfies

$$|\psi_i(E,\vec{k}_{\parallel},d)|^2 = \frac{|\psi_i^0(E,\vec{k}_{\parallel},d)|^2}{|1-U_0 G_0^R(d,d,\vec{k}_{\parallel},E)|^2}, \quad i=L,R$$

$$\cong |\psi_i^0(E,\vec{k}_{\parallel},d)|^2\left(1+\pi\frac{(\hbar^2/mK_0^2)^2}{\gamma_{\rm WKB}}\delta(E_\perp-E_r)\right). \tag{21}$$

In Eq. (21), the symbol ψ^0 represents the extended-basis function of the average-barrier potential in the absence of the impurity, and we have used the "sharp-resonance approximation" [Eq. (18)] to write the second line. Inserting Eq. (21) into the definition of the self-energy in Eqs. (10) yields the result that the self-energy now has two parts, one nonresonant and one resonant:

$$\Sigma(E) = \Sigma^{\rm nr}(E) + \Sigma^{\rm res}(E), \tag{22a}$$

$$\Sigma^{\rm res}(E) = \Sigma_L^{\rm res} + \Sigma_R^{\rm res}(E). \tag{22b}$$

The quantity $\Sigma^{\rm nr}$ is the nonresonant self-energy discussed in Sec. V C. The resonant self-energy $\Sigma^{\rm res}$, which contains both left ($\Sigma_L^{\rm res}$) and right ($\Sigma_R^{\rm res}$) parts, results from inserting the δ-function term in Eq. (21) into Eqs. (6b) and (6c).[18,85]

When the resonance energy E_r moves below the Fermi level (i.e., ζ_L in $\Sigma_L^{\rm res}$ and $\zeta_L - eV$ in $\Sigma_R^{\rm res}$), large threshold structure appears at energy equal to $-\hbar\omega_0$ below the Fermi level. Thus, as in the case of resonant-elastic tunneling we can regard the resonance as a switch. When the resonance energy passes the Fermi level it either opens (if it is moving below) or closes (if it is moving above) a "window" for electrons to pass through.

The total conductance, derived from Eqs. (8), contains three dominant contributions,[18]

$$G = \frac{dJ(eV)}{d(eV)} = G_0(eV) + G_{\rm nr}(eV) + G_{\rm res}(eV). \tag{23}$$

The quantities G_0 and $G_{\rm nr}$ are, respectively, the resonant-elastic conductance described in Sec. V B and the nonresonant-inelastic conductance described in Sec. V C. The resonant-inelastic conductance $G_{\rm res}$, at $T=0$, is defined by[18,85]

$$G_{\rm res} \equiv \frac{dJ_{\rm res}(eV)}{d(eV)}, \tag{24a}$$

$$J_{\rm res}(eV) = \frac{2e}{h}\int_{\zeta_L-eV}^{\zeta_L} dE \int \frac{d^2k_{\parallel}}{(2\pi)^2}\left[|S_{12}(E,\vec{k}_{\parallel})|^2 - S_{12}^0(E,\vec{k}_{\parallel})|^2\right]$$
$$\times\{2[G_1(E,\vec{k}_{\parallel}) - G_1^0(E,\vec{k}_{\parallel}) + U_0|G_0^R(d,d,\vec{k}_{\parallel},E)|^2]\Sigma_1^{\rm res}(E)$$
$$- [G_2(E,\vec{k}_{\parallel}) - G_2^0(E,\vec{k}_{\parallel})]\Sigma_2^{\rm res}(E)\}. \tag{24b}$$

Quantities with superscript zero correspond to the average barrier in the absence of impurities. The resonant-inelastic conductance $G_{\rm res}$ is illustrated schematically in Fig. 17. The quantities F_L and F_R in Fig. 17 are the "strengths" of $\Sigma_L^{\rm res}$ and $\Sigma_R^{\rm res}$, respectively; that is, $F_L > F_R$ if $|\psi_L^0(E_r)| > |\psi_R^0(E_r)|$. The behavior of $G_{\rm res}$ can be understood in a simple fashion by applying our concept of the resonance as

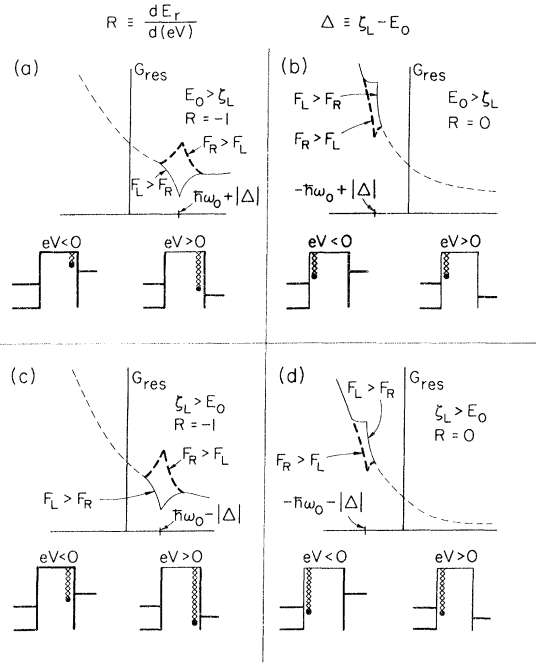

FIG. 17. Schematic illustration of the resonant-inelastic conductance. F_L and F_R are the strengths of the left and right resonant self-energies, respectively. Upon comparing Fig. 17 with Fig. 15, we see that resonant-inelastic tunneling occurs. Thus, in Figs. 17(a) and (c), phonon structure appears in forward bias alone, while in Figs. 17(b) and (d), phonon structure appears in reverse bias alone. The schematic tunnel junctions in the figure illustrate the switch concept. The black dot represents the resonance energy and the cross hatching indicates the range of energies for which resonant tunneling can occur (after Kleiman, Ref. 18).

a switch. From Eq. (24b), we see that the resonant-inelastic conductance contains the convolution of the resonant parts of both $|S_{12}|^2$ and Σ. It is the resonant portion of $|S_{12}|^2$ which produces the switch behavior in the resonant conductance of Eq. (19). Both the elastic switch in $|S_{12}|^2$ and the inelastic switch in $\Sigma^{\rm res}$ must be open for the conductance $G_{\rm res}$ to exhibit structure due to inelastic processes. Therefore, phonon-induced fine structure in $G_{\rm res}$ appears only when the resonant-elastic channel is already open. The consequences of this result are displayed in Fig. 17.

From Fig. 17 we see that resonant-impurity-assisted-inelastic tunneling for $R \cong -1$ predicts large enhancements of the "forward"-bias cusp structure at the phonon energies. Precisely this phenomenon is observed in an enormous variety of semiconductor junctions.[10,11,19–24,26–30] We observe it in the data shown in Figs. 4, 5, 9, 10, and 11. A mild asymmetry of this kind is predicted by bulk electron-phonon coupling which is abruptly terminated at the edge of the semiconductor in a metal-insulator junction.[35] However, the predicted bulk effect is small, and certainly cannot describe the large asymmetry in the photosensitive inelastic channel described in Sec. III. Therefore the asymmetry in the inelastic line shape as well as the zero-bias conductance minimum observed in our GaAs : Zn, Au-Ge p-n junctions leads to the identification of resonant trap-assisted tunneling as the new "channel" cut on by the photoexcitation of the Au-Ge complex.

A final instructive example is that described by Schein and Compton[93] who reported characteristic phonon line shapes on metal-oxide p- and n-type silicon junctions. They found that P impurities which were diffused into Si : B samples always produced larger phonon structure in the sign of the bias in which the semiconductor majority carriers tunnel [i.e., when the P implanation resulted in a $p(n)$-type substrate, the large structure occurred in forward (reverse) bias, in the conventions of Fig. 13.] The phonon asymmetry was invariably accompanied by ZBA.

We can apply the qualitative static and dynamic resonant δ-function models developed in Secs. V B and V D, respectively, to interpret this phonon asymmetry. The model predicts dominance of the phonon cusp structure for majority-carrier injection into the metal if $R \equiv d[V(d)/d(eV)] = -1$, where $V(x)$ is the average-barrier potential, and d is the resonant-impurity position. Also, if $-\frac{1}{2} \gtrsim R \gtrsim -1$, it predicts zero-bias conductance minima if E_0, the zero-bias resonance energy of Eqs. (20), is greater than the semiconductor Fermi degeneracy ζ_L. An additional requirement for compatibility of Fig. 17 with Schein and Compton's experiment is that F_L must be greater than F_R (i.e., the "strength" of the left-resonant self-energy must be greater than that of the right). In order to make a microscopic identification of our model with experiment, we must determine both d and R from the average-barrier potential. In order for resonant-trap states to affect the tunneling characteristics, not only must $T_L \simeq T_R$, but also the resonance energy must be low enough for tunneling charge carriers to "see" the resonance: This immediately eliminates shallow impurities as possible sources of the resonances near zero bias. Deep traps at the semiconductor oxide interfact in a typical metal-oxide semiconductor junction, however, can be resonant. Surface states at this interface are known[94] to provide attractive potentials for the majority carriers if strong depletion regions exist in the semiconductor prior to the oxide interface. Charge accumulation in these potentials also would require $R \cong -1$ by forcing most of the applied-voltage drop across the semiconductor depletion region. Finally a slight detuning of the traps from exact resonance easily can occur and force $F_L > F_R$ (i.e., $T_L > T_R$). Finally, as Schein and Compton's units also exhibited ZBA (conductance minima), we

have all of the ingredients for an interpretation of their observed LO-phonon line shapes as being caused by resonant-inelastic tunneling via trap states, possibly surface states,[94] in the semiconductor electrode but near the oxide interface. Concerning their local-mode-phonon line shapes, however, Schein and Compton suggest that the observation only of majority-carrier-dopant local modes implicates charged dopant impurities at the semiconductor edge of the space-charge region. This would be inconsistent with the $R=-1$ requirement in our model. However, the observation of only majority-carrier-dopant local modes also could be a consequence of impurity segregation at the oxide interface during the rather brutal fabrication of the junctions.

VI. SYNOPSIS

The thrust of the studies reported in this paper is the documentation and application of the concept that the physical mechanisms of electron tunneling in a given junction depend upon the potential-energy profile (i.e., dopant and defect distributions) in that junction. Perhaps surprisingly, we find that in the case of good junctions, resonant- ("two-step") tunneling processes predominate for thicker junctions and not in thin ones for which dopant fluctuation phenomena initially were anticipated to be significant.[24,29] In the thinner junctions on heavily doped substrates, the average-barrier model seems to describe the measurements quite adequately.

We have documented the occurrence of a change in tunneling mechanism as a function of substrate doping by studying Au-Ge alloy diodes on GaAs : Zn substrates (Sec. III). For $p=5.4\times10^{19}$ cm^{-3} ($n\simeq1\times10^{19}$ cm^{-3}) the average-barrier model describes the data quite well. However, for $p=1.3\times10^{19}$ cm^{-3} ($n\simeq6\times10^{18}$ cm^{-3}), the average-barrier model predictions fail to describe the data and, in addition, the tunnel characteristics become photosensitive. Our examination of the photosensitive phenomena has led to the interpretation that essentially all of the current in these diodes is "assisted" by Au-Ge complexes which upon photoexcitation become trap states causing both resonant-elastic and resonant-inelastic tunneling. This interpretation is buttressed by the development of a new theory of both phenomena[17,18] whose results have been outlined in Sec. V for the case of a simple model. In Sec. V the theory has been applied to describe such phenomena in a variety of tunnel junctions, thereby permitting us to extend the insight obtained for our study of GaAs (Zn : Au-Ge) to the characterization of other systems. Such a characterization of defect structure and phonon dispersion in III-V mixed-crystal alloy diodes ($Ga_{1-x}Al_xAs$, $GaAs_{1-x}P_x$, and $In_{1-x}Ga_xP$) has been described in Sec. IV.

This work has led to two substantial changes in our perspective about tunneling in semiconductors. First, the long-standing discrepancy[1] between the experimental measurements of the tunnel characteristics in p-n diodes and predictions of the one-electron average-barrier models of these diodes has been resolved. All of the early studies[1] led to this discrepancy because they were performed on units which either were too lightly doped or contained too many defects for average-barrier tunneling to be the dominant current-flow mechanism. Indeed, those units on which low-temperature (4.2 °K) measurements have been available all show the zero-bias conductance minima and highly asymmetric optical-phonon-induced fine structure which signal the occurrence of resonant impurity-assisted tunneling. Second, our studies of III-V mixed-crystal alloy diodes have provided a key insight into the effect of lattice-mismatch defects on the characteristics of junctions. We have established that alloy regrowth on mixed crystals whose components exhibit substantial lattice mismatch (e.g., $In_{1-x}Ga_xP$) upsets the "ordered" crystal lattices in mixed crystals thereby leading to numerous defects. These defects in turn cause resonant tunneling to dominate the current characteristics of tunnel diodes, and in the case of light-emitting diodes reduce the efficiency. Thus, in retrospect, the lack of success over the years on the part of various groups (including our own) in fabricating good tunnel and light-emitting diodes using certain mixed-crystal alloys not only can be understood, but by the selection of suitable crystal systems and adjustment of the junction fabrication techniques[70] often can be mitigated or eliminated.

ACKNOWLEDGMENTS

We are indebted to Dr. W. D. Compton, Dr. D. Cullen, Dr. L. C. Davis, and Dr. L. Schein for numerous discussions about impurity-assisted tunneling. We also thank G. W. Zack, R. D. Burnham, H. M. Macksey, K. A. Kuehl, Yuri S. Moroz, and V. Swanson for technical assistance. In addition we are grateful to J. B. Woodhouse for taking the electron-microprobe data; M. M. Blouke (Texas Instruments, Dallas) for providing the Ge : Hg detector; J. W. Burd, M. G. Craford, and F. V. Williams (Monsanto, St. Louis) for some of the crystals used in this work; and the University of Illinois Industrial Affliates Program for supplying some of the equipment.

*Work supported in part by the Advanced Research Projects Agency under Contract No. HC 15-67-C-0221, by the National Science Foundation under Grant No. GK-18960, and by the Joint Services Electronics Program under Contract No. DAAB-07-67-C-0199.

†Also, member of technical staff, Bell Telephone Lab-

oratories (doctoral-support plan).

[1]C. B. Duke, *Tunneling in Solids* (Academic, New York, 1969).

[2]C. B. Duke, J. Vac. Sci. Technol. 7, 22 (1970).

[3]F. Steinrisser, L. C. Davis, and C. B. Duke, Phys. Rev. 176, 912 (1968).

[4]L. C. Davis and F. Steinrisser, Phys. Rev. B1, 614 (1970).

[5]P. Guétin and G. Schréder, Phys. Rev. Letters 27, 326 (1971).

[6]I. Giaever and H. R. Zeller, Phys. Rev. Letters 20, 1504 (1969).

[7]H. R. Zeller and I. Giaever, Phys. Rev. 181, 789 (1969).

[8]G. H. Parker and G. A. Mead. Appl. Phys. Letters 14, 21 (1969); Phys. Rev. 184, 780 (1969).

[9]C. B. Duke, G. G. Kleiman, A. M. Andrews, R. D. Burnham, N. Holonyak, Jr., and H. W. Korb, in *Proceedings of the Tenth International Conference on the Physics of Semiconductors, Cambridge, Mass.*, 1970 (U. S. AEC, Oak Ridge, Tenn., 1970).

[10]D. E. Cullen, E. L. Wolf, and W. Dale Compton, Phys. Rev. B2, 3157 (1970).

[11]L. B. Schein and W. Dale Compton, Appl. Phys. Letters 17, 236 (1970).

[12]M. N. Alexander and D. F. Holcomb, Rev. Mod. Phys. 40, 815 (1968).

[13]E. L. Wolf, D. L. Losee, D. E. Cullen, and W. Dale Compton, Phys. Rev. Letters 26, 438 (1971).

[14]N. A. Mora, S. Bermon, and J. J. Loferski, Phys. Rev. Letters 27, 664 (1971).

[15]A. D. Brailsford and L. C. Davis, Phys. Rev. B2, 1708 (1970).

[16]L. C. Davis, Phys. Rev. B2, 1714 (1970).

[17]C. B. Duke and G. G. Kleiman, Rev. Phys. Appl. 5, 906 (1970).

[18]G. G. Kleiman, Ph. D. thesis (University of Illinois, 1971) (unpublished).

[19]R. N. Hall, J. H. Racette, and H. Ehrenreich, Phys. Rev. Letters 4, 436 (1960).

[20]R. N. Hall, in *Proceedings of the International Conference on Semiconductor Physics, Prague*, 1960 (Academic, New York, 1969), p. 193.

[21]R. N. Hall and J. H. Racette, J. Appl. Phys. Suppl. 32, 2078 (1961).

[22]B. M. Vul, E. I. Zavaritskaya, and N. V. Zavaritskii, Fiz. Tverd. Tela 8, 888 (1966) [Sov. Phys. Solid State 8, 710 (1966)]; J. Phys. Soc. Japan Suppl. 21, 598 (1966).

[23]G. D. Mahan and J. W. Conley, Appl. Phys. Letters 11, 29 (1967).

[24]J. W. Conley and G. D. Mahan, Phys. Rev. 161, 681 (1967).

[25]C. B. Duke, S. D. Silverstein, and A. J. Bennett, Phys. Rev. Letters 19, 312 (1967); Phys. Rev. 176, 969 (1968).

[26]D. C. Tsui, Phys. Rev. Letters 21, 994 (1968).

[27]C. B. Duke, M. J. Rice, and F. Steinrisser, Phys. Rev. 181, 733 (1969).

[28]M. Mikkor and W. C. Vassel, Phys. Rev. B 2, 1975 (1970).

[29]D. L. Losee and E. L. Wolf, Phys. Rev. 187, 925 (1969).

[30]Z. Stroubek, Solid State Commun. 7, 1561 (1969); Phys. Rev. B2, 3170 (1970).

[31]K. W. Johnson and D. H. Olson, Phys. Rev. B3, 1244 (1971).

[32]H. W. Korb, A. M. Andrews, N. Holonyak, Jr., R. D. Burnham, C. B. Duke, and G. G. Kleiman, Solid State Commun. 9, 1531 (1971).

[33]L. C. Davis and C. B. Duke, Phys. Rev. 184, 764 (1969).

[34]C. B. Duke and G. G. Kleiman, Phys. Rev. B2, 1270 (1970).

[35]L. C. Davis, Phys. Rev. B2, 4943 (1970).

[36]C. B. Duke and M. E. Alferieff, J. Chem. Phys. 46, 923 (1969).

[37]C. M. Wolfe, C. J. Nuese, and N. Holonyak, Jr., J. Appl. Phys. 36, 3790 (1965).

[38]C. J. Nuese, G. E. Stillman, M. D. Sirkis, and N. Holonyak, Jr., Solid State Electron. 9, 735 (1966).

[39]R. D. Burnham, N. Holonyak, Jr., D. L. Keune, D. R. Scifres, and P. D. Dapkus, Appl. Phys. Letters 17, 430 (1970).

[40]W. R. Patterson and J. Shewchun, Rev. Sci. Instr. 35, 1704 (1964).

[41]H. W. Korb and N. Holonyak, Jr., Rev. Sci. Instr. (to be published).

[42]J. A. Copeland, IEEE Trans. Electron. Devices ED-18, 50 (1971).

[43]C. B. Duke, *Tunneling in Solids* (Academic, New York, 1969), Sec. 13 and 14.

[44]E. L. Wolf and D. L. Losee, Phys. Rev. B2, 3660 (1970).

[45]N. Holonyak, Jr., D. L. Keune, R. D. Burnham, and C. B. Duke, Phys. Rev. Letters 24, 589 (1970).

[46]L. B. Valdes, *The Physical Theory of Transistors* (McGraw-Hill, New York, 1961).

[47]D. J. BenDaniel and C. B. Duke, Phys. Rev. 152, 863 (1966).

[48]Typical capacitance measurements are presented in the following articles: B. Pelligrini, Solid State Electron. 13, 1175 (1970); T. Arizumi and A. Yoshida, Japan. J. Appl. Phys. 7, 748 (1968); T. Arizami, T. Wada, and A. Yoshida, *ibid.* 4, 415 (1965); D. J. Dumin and G. L. Pearson, J. Appl. Phys. 36, 3418 (1965); H. K. Gummel and D. L. Scharfetter, *ibid.* 38, 2148 (1967).

[49]T. N. Morgan, Phys. Rev. 148, 890 (1966).

[50]W. Bernard, H. Roth, A. P. Schmid, and P. Zeldes, Phys. Rev. 131, 627 (1963).

[51]C. T. Sah, in *Tunneling Phenomena in Solids*, edited by E. Burnstein and S. Lundqvist (Plenum, New York, 1969), p. 193.

[52]L. Esaki, in Ref. 51, p. 47.

[53]I. Gaiever, Phys. Rev. Letters 20, 1286 (1968).

[54]R. N. Hall and N. Holoyak, Jr., U. S. Patent No. 3417248, 1968.

[55]E. W. Plummer and R. D. Young, Phys. Rev. B1, 2088 (1970).

[56]L. V. Keldysh and Yu. V. Kopaev, Fiz. Tverd. Tela 5, 1411 (1963) [Sov. Phys. Solid State 5, 1026 (1963)]. For a correction of errors in this analysis, see G. D. Mahan and C. B. Duke, Phys. Rev. 149, 705 (1966).

[57]C. B. Duke, A. M. Andrews, R. D. Burnham, N. Holonyak, Jr., and H. W. Korb, Rev. Phys. Appl. 5, 906 (1970).

[58]T. Carruthers, Appl. Phys. Letters 18, 35 (1971).

[59]A. van der Ziel, *Fluctuations Phenomena in Semiconductors* (Butterworths, London, 1959), p. 22–45.

[60]A. M. Andrews, Ph. D. thesis (University of Illinois, 1971) (unpublished).

[61]L. J. van der Pauw, Phillips Res. Rept. 13, 1 (1958).

[62]F. E. Rosztoczy, F. Ermanis, I. Hayashi, and B. Schwartz, J. Appl. Phys. 41, 264 (1970).

[63]C. B. Duke, *Tunneling in Solids* (Academic, New York, 1969), Sec. 20.

[64]D. Cullen, Ph. D. thesis (University of Illinois, 1907) (unpublished).

[65]Zh. I. Alfërov, M. V. Andreev, D. Z. Garbuzov, Ju. V. Zhilyaev, E. P. Morozov, E. L. Portnoi, and V. G. Trofim, Fiz. Tech. Poluprov. 4, 1826 (1970) [Sov. Phys. Semicond. 4, 1573 (1971)].

[66]I. Hayashi, M. B. Panish, P. W. Foy, and S. Sumski, Appl. Phys. Letters 17, 109 (1970).

[67]N. Holonyak, Jr. and S. F. Bevacqua, Appl. Phys. Letters 1, 82 (1962).

[68]W. O. Groves, A. H. Herzog, and M. G. Craford, Appl. Phys. Letters 19, 184 (1971).

[69]N. Holonyak, Jr., D. R. Scifres, R. D. Burnham, M. G. Craford, W. O. Groves, and A. H. Herzog, Appl. Phys. Letters 19, 254 (1971).

[70]H. M. Macksey, N. Holonyak, Jr., D. R. Scifres, R. D. Dupuis, and G. W. Zack, Appl. Phys. Letters (to be published).

[71]M. Ilegems and G. L. Pearson, Phys. Rev. B1, 1576 (1970).

[72]H. W. Verleur and A. S. Barker, Phys. Rev. 149, 715 (1966).

[73]Y. S. Chen, W. Shockley, and G. L. Pearson, Phys. Rev. 151, 648 (1966).

[74]G. Lucovsky, M. H. Brodsky, and E. Burstein, Phys. Rev. B2, 3295 (1970).

[75]H. C. Casey, Jr. and F. A. Trumbore, Mater. Sci. Eng. 6, 69 (1970), give primary reference for lattice constant measurements.

[76]A. G. Chynoweth, W. L. Feldman, and R. A. Logan, Phys. Rev. 121, 684 (1961).

[77]R. S. Claassen, J. Appl. Phys. 32, 2372 (1961).

[78]Zh. I. Alfërov, D. Z. Garbuzov, V. A. Grigor'eva, Yu. V. Zhilyaev, L. V. Kradinova, V. I. Korlkov, E. P. Morozov, O. A. Ninua, E. L. Portnoi, V. D. Prochukan, and M. K. Trukan, Fiz. Tverd. Tela 9, 279 (1967) [Sov. Phys. Solid State 9, 208 (1967)].

[79]M. G. Craford, W. O. Groves, and M. F. Fox, J. Electrochem. Soc. 118, 355 (1971).

[80]I. F. Chang and S. S. Mitra, Phys. Rev. B2, 1215 (1970).

[81]I. F. Chang and S. S. Mitra, Phys. Rev. 172, 924 (1968).

[82]C. B. Duke, Phys. Rev. 186, 588 (1969).

[83]M. H. Brodsky, G. Lucovsky, M. F. Chen, and T. S. Plaskett, Phys. Rev. B2, 3303 (1970).

[84]R. A. Logan, P. J. Dean, H. G. White, and W. Wiegmann, J. Appl. Phys. 42, 2328 (1971).

[85]G. G. Kleiman and C. B. Duke (unpublished).

[86]J. W. Gadzuk, J. Appl. Phys. 41, 286 (1970).

[87]J. A. Appelbaum and W. F. Brinkman, Phys. Rev. 186, 464 (1969); B2, 907 (1970).

[88]J. G. Adler, H. J. Kreuzer, and W. J. Wattamaniuk, Phys. Rev. Letters 27, 185 (1971).

[89]A. A. Abrikosov, L. P. Gorkov, and I. E. Dzyaloshinski, *Methods of Quantum Field Theory in Statistical Physics* (Prentice-Hall, Englewood Cliffs, N. J., 1963).

[90]A. J. Bennett and C. B. Duke, Phys. Rev. 160, 541 (1967).

[91]L. D. Landau and E. M. Lifschitz, *Quantum Mechanics* (Pergamon, London, 1958).

[92]I. Adawi, Phys. Rev. 143, A788 (1964).

[93]L. Schein and W. D. Compton, Phys. Rev. B4, 1128 (1971).

[94]Numerous references on surface states are contained in the article by S. G. Davison and J. D. Levine, in *Solid State Physics*, edited by F. Seitz and D. Turnbull (Academic, New York, 1966), Vol. 25, p. 1.

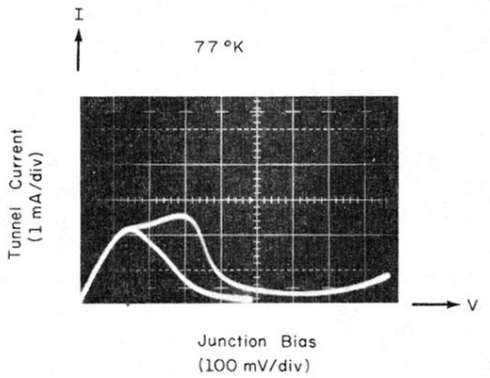

FIG. 2. *I-V* curve-tracer plot at 77 °K of a GaAs(Zn: Au-Ge) tunnel diode. The lower trace is obtained in the dark. The upper trace is obtained after saturation of changes in characteristics with the radiation output of a tungsten lamp.